Collaborative Scheduling of Time-dependent UAVs, Vehicles and Workers for Crowdsensing in Disaster Response

LEI HAN, Xidian University, China
JINHAO ZHANG, Xidian University, China
JINHUI LIU*, Xidian University, China
ZHIYONG YU, Fuzhou University, China
LIANG WANG, Northwestern Polytechnical University, China
QUAN WANG, Xidian University, China
ZHIWEN YU, Harbin Engineering University, China

Frequent natural disasters cause significant losses to human society, and timely, efficient collection of post-disaster environmental information is the foundation for effective rescue operations. Due to the extreme complexity of post-disaster environments, existing sensing technologies such as mobile crowdsensing suffer from weak environmental adaptability, insufficient professional sensing capabilities, and poor practicality of sensing solutions. Therefore, this paper explores a heterogeneous multi-agent online collaborative scheduling algorithm, HoCs-MPQ, to achieve efficient collection of post-disaster environmental information. HoCs-MPQ models collaboration and conflict relationships among multiple elements through weighted undirected graph construction, and iteratively solves the maximum weight independent set based on multi-priority queues, ultimately achieving collaborative sensing scheduling of time-dependent UAVs, vehicles, and workers. Specifically, (1) HoCs-MPQ constructs weighted undirected graph nodes based on collaborative relationships among multiple elements and quantifies their weights, then models the weighted undirected graph based on conflict relationships between nodes; (2) HoCs-MPQ solves the maximum weight independent set based on iterated local search, and accelerates the solution process using multi-priority queues. Finally, we conducted detailed experiments based on extensive real-world and simulated data. The experiments show that, compared to baseline methods (e.g., HoCs-GREEDY, HoCs-K-WTA, HoCs-MADL, and HoCs-MARL), HoCs-MPQ improves task completion rates by an average of 54.13%, 23.82%, 14.12%, and 12.89% respectively, with computation time for single online autonomous scheduling decisions not exceeding 3 seconds.

Additional Key Words and Phrases: Mobile crowdsensing, Multi-agent collaborative sensing, Collaborative sensing scheduling, Weighted undirected graph, Maximum weight independent set.

ACM Reference Format:

Authors' Contact Information: Lei Han, hanlei@xidian.edu.cn, Xidian University, Xi'an, China; Jinhao Zhang, z1028406171@163.com, Xidian University, Xi'an, China; Jinhui Liu, jhliu@mail.xidian.edu.cn, Xidian University, Xi'an, China; Zhiyong Yu, yuzhiyong@fzu.edu.cn, Fuzhou University, Fuzhou, China; Liang Wang, liangwang@nwpu.edu.cn, Northwestern Polytechnical University, Xi'an, China; Quan Wang, qwang@xidian.edu.cn, Xidian University, Xi'an, China; Zhiwen Yu, zhiwenyu@nwpu.edu.cn, Harbin Engineering University, Harbin, China.

Permission to make digital or hard copies of all or part of this work for personal or classroom use is granted without fee provided that copies are not made or distributed for profit or commercial advantage and that copies bear this notice and the full citation on the first page. Copyrights for components of this work owned by others than the author(s) must be honored. Abstracting with credit is permitted. To copy otherwise, or republish, to post on servers or to redistribute to lists, requires prior specific permission and/or a fee. Request permissions from permissions@acm.org.

@ 2018 Copyright held by the owner/author(s). Publication rights licensed to ACM. ACM 2476-1249/2018/8-ART111

^{*}Corresponding author.

1 Introduction

According to the 2023 Global Natural Disaster Assessment Report [1], there were 326 large-scale natural disasters globally in 2023, causing 86,473 deaths and direct economic losses of up to \$202.652 billion. To reduce the severe impact of natural disasters, it is crucial to organize post-disaster rescue operations efficiently and promptly. Accurate and real-time situational awareness is the foundation for effective rescue actions [35].

Currently, mainstream situational awareness approaches include wireless sensor networks (WSNs) [12, 48] and mobile crowdsensing (MCS) [19, 58]. However, these technologies have limitations in post-disaster scenarios. WSNs rely on pre-deployed static sensors and lack adaptability in complex and dynamic environments. MCS uses people with portable smart devices as sensing units. Although it is more adaptable and requires less infrastructure, human mobility is limited in disaster settings, and portable devices lack sensing professionalism.

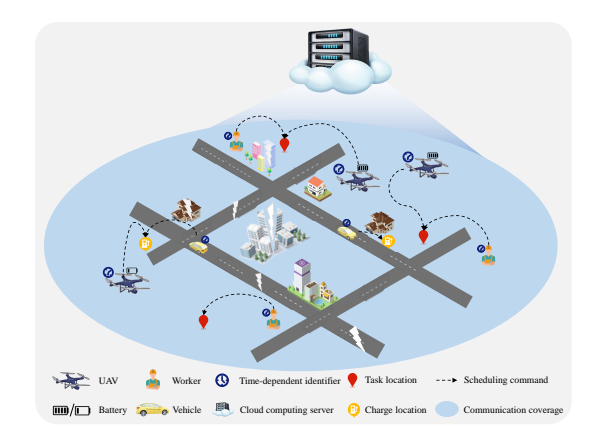
In recent years, UAVs have played an increasingly important role in disaster response. UAVs are highly mobile, easy to deploy, and capable of carrying professional sensors [29, 51, 52, 74]. However, current studies on UAV-based data collection often rely on two overly optimistic assumptions: (1) UAVs can autonomously collect data; however, the complex post-disaster environment severely constrains the UAVs' mobility, which drastically impairs their sensing capabilities.(2) UAVs can automatically recharge at charging stations. In reality, such stations are rare in cities and may be damaged after disasters. It is also difficult for UAVs to connect to power without assistance in outdoor environments.

In recent years, with the widespread adoption and application of UAVs, new energy vehicles, and portable smart terminals, their complementary advantages have offered potential solutions to the aforementioned problems. Specifically, as shown in Fig. 1a, UAVs possess controlled autonomy, superior mobility, and the flexibility to carry professional sensing equipment[39]. Combined with the charging and endurance capabilities of new energy vehicles [57] and the agile control capabilities of portable smart terminals [15], and further aided by UAV flight control takeover platforms [8], we can effectively achieve efficient post-disaster environmental data collection[13]. Building upon this collaborative approach, a recent study [14] leverages the heterogeneity and collaboration of UAVs, vehicles, and workers to collect environmental data efficiently. As shown in Fig. 1b, workers can use portable devices to control UAVs for agile data collection. Vehicles can act as mobile charging stations for UAVs with low power. However, this study still has two limitations: (1) Since natural disasters are highly unpredictable, it is hard to model training environments. Learning-based solutions are difficult to apply in real post-disaster scenarios. (2) The proposed solution assumes fixed coupling among UAVs, vehicles, and workers, while in reality, their relationships are time-dependent.

This paper studies the collaborative scheduling of time-dependent UAVs, vehicles, and workers for crowdsensing in disaster response. We have two goals: (1) Propose an online heterogeneous multi-agent collaborative scheduling algorithm that does not require modeling training environments. (2) Effectively schedule time-dependent UAVs, vehicles, and workers to complete post-disaster data collection tasks efficiently. To realize the aforementioned goals, we face two main challenges: (1) The five-dimensional matching problem involving UAVs, vehicles, workers, task points, and charging points is very complex. It is a challenge to model the problem accurately to reflect the complex logical relationships. (2) Solving the five-dimensional matching problem requires high computation and must consider resource and time constraints to ensure timely decisions in dynamic environments.

To address these challenges, we propose a heterogeneous multi-agent online collaborative scheduling algorithm based on weighted undirected graph modeling and maximum weight independent set solution, named HoCs-MPQ. (1) We model the five-dimensional matching problem as a maximum weight independent set (MWIS) problem on a weighted undirected graph. The nodes and edges represent collaborative and conflictual relationships among agents (e.g., UAVs, vehicles, and workers). By solving the MWIS, we maximize the collaboration among UAVs, vehicles, and workers. (2) As the graph is dense, we use multiple queues to store the core nodes, reducing the size





- (a) Illustration of UAVs, vehicles, and workers with a takeover platform
- (b) Example of collaboration among time-dependent UAVs, vehicles, and workers.

Fig. 1. Collaboration Among Time-Dependent UAVs, Vehicles, and Workers.

of the graph while retaining key information. We then iteratively read nodes from the queues to optimize the MWIS solution and shorten computation time.

Our main contributions are as follows:

- To the best of our knowledge, this work is the first research addressing the collaborative scheduling of time-dependent UAVs, vehicles, and workers for crowdsensing in disaster response. We also prove that the problem is NP-Hard.
- To tackle the aforementioned issues, we propose an online heterogeneous multi-agent collaborative scheduling algorithm, named HoCs-MPQ. (1) HoCs-MPQ models collaborative and conflictual relationships among agents through a weighted undirected graph. (2) HoCs-MPQ uses multi-priority queues to speed up the solution of the maximum weight independent set as the result of heterogeneous multi-agent collaborative scheduling.
- We conducted detailed experiments using real-world and simulated data. Compared with the baseline algorithms HoCs-GREEDY, HoCs-K-WTA, HoCs-MADL, and HoCs-MARL, HoCs-MPQ improves the task completion rate by 54.13%, 23.82%, 14.12%, and 12.89%, respectively. The single matching decision time does not exceed 3 seconds on any dataset. The experimental code and data examples for this study can be referenced in [5].

The contents of this paper are arranged as follows: Section 2 discusses some related works; Section 3 formulates the problem of collaborative scheduling of time-dependent UAVs, vehicles and workers for crowdsensing in disaster response; Section 4 provides a comprehensive and detailed description of the proposed HoCs-MPQ method; then the experiments are conducted in Section 5; finally, conclusions and future work are summarized in Section 6.

Related Work

The properties and functions of heterogeneous agents such as UAVs, vehicles, and workers vary significantly. Their collaboration modes are also diverse. Existing studies on heterogeneous multi-agent collaboration can be classified into three types: (1) Heterogeneous multi-agent collaborative sensing based on spatial division; (2) Heterogeneous multi-agent collaborative sensing based on task-phase division; (3) Heterogeneous multi-agent collaborative sensing based on fine-grained coordination.

2.1 Heterogeneous Multi-Agent Collaborative Sensing Based on Spatial Division

In this collaborative sensing mode, heterogeneous agents collect data at different spatial locations according to their mobility differences. This collaboration can be divided into three types. First, the most common type is the collaboration between UAVs and vehicles based on spatial separation. For example, Wu et al. [60] planned joint paths for UAVs and vehicles, aiming to minimize global sensing time through high-altitude and ground-level deployment. In the field of navigation, Zuo et al. [75] used UAVs to collect ground information from the air to assist vehicle navigation in complex environments. Zang et al. [66] aimed to reduce collision risks among large-scale vehicle fleets by using UAVs to collect ground-level information from high altitudes. In terms of collaborative mapping between UAVs and vehicles, some works used UAVs to provide large-scale aerial data while vehicles filled in ground-level details [4, 18, 21, 36]. Second, some studies focus on UAV/vehicle and human collaboration based on spatial separation. For example, Ding et al. [7] constructed a low-cost urban sensing system by leveraging the spatial distribution differences between human crowds and autonomous vehicles. Zheng et al. [72] studied how UAVs and humans could search different areas simultaneously to efficiently locate fugitives. In emergency response scenarios, Minaeian et al. [38] explored how UAVs at high altitudes could assist ground patrols by providing real-time feedback on suspicious targets. Finally, a few works investigate the spatial collaboration among UAVs, vehicles, and humans. For example, Wu et al. [59] dispatched small UAVs, intelligent connected vehicles, and human groups to different areas to search for multiple ground targets.

2.2 Heterogeneous Multi-Agent Collaborative Sensing Based on Task-phase Division

In this collaborative sensing mode, the task is divided into multiple sub-tasks at different stages, and heterogeneous agents complete each sub-task in sequence according to their functional characteristics. First, the most common mode is the collaboration between UAVs and vehicles in task-phase division. For example, studies [42, 45] used UAVs to perform fast area exploration and mark points of interest, and then used unmanned vehicles to conduct precise target detection. Wang et al. [57] focused on how to use vehicles as UAV carriers to extend their range, in order to perform long-duration monitoring tasks. Based on the strong transport capacity of trucks and the precise delivery ability of UAVs, Luo et al. [33] realized a two-stage delivery system using trucks and UAVs.Similarly, Fu et al. [10] used UAVs to collect data and ground vehicles to transmit the collected data, aiming to balance high-efficiency data collection and processing. Second, some studies focus on UAV/vehicle and worker collaboration in task-phase division. For example, Niroui et al. [41] used UAVs to capture aerial images of disaster areas and transmit them in real time to human-operated devices. Then, humans marked key targets using augmented reality (AR). In the field of construction engineering, Krizmancic et al. [20] used UAVs to perform aerial scanning tasks, while humans conducted semantic analysis and material transport. In power inspection scenarios, Zheng et al. [73] used UAVs to detect transmission faults and inform operators for repair of power facilities. To enable rapid search for missing tourists, Xu et al. [61] proposed a two-stage model where UAVs conduct detection and rescue workers carry out search and rescue, greatly improving the efficiency of the mission. Finally, some studies involve three-agent collaboration across phases. Ghassemi et al. [11] proposed a three-stage model: UAVs scan the area, vehicles deliver supplies, and workers coordinate operations.

2.3 Heterogeneous Multi-Agent Collaborative Sensing Based on Fine-grained Coordination

In this collaborative sensing mode, heterogeneous agents achieve fine-grained cooperation on specific tasks by leveraging their diverse capabilities and synergies. First, the most common fine-grained collaboration mode is between UAVs and vehicles. Hu et al. [16] proposed a 3D cooperative detection framework, CoCa3D, which enables real-time sharing of critical data between UAVs and vehicles through deep uncertainty estimation. Wang et al. [54] jointly optimized the trajectories of UAVs and vehicles to maintain line-of-sight tracking, addressing the problem of UAV-based monitoring being blocked by obstacles in urban environments. Zhao et al. [69] proposed a

novel goal-oriented MADRL framework named gMADRL-VCS, where UGVs act as UAV carriers for road transport and charging, while UAVs navigate to collect post-disaster data. The system simultaneously learns the routing policy of UAVs and the navigation strategy of UGVs. Second, some studies explore fine-grained collaboration between UAVs/vehicles and humans. To address the challenge of heterogeneous multi-agent sensing caused by communication redundancy and transmission delay, one study [62] used UAV-based semantic communication to transmit high-quality feature information to humans, supporting real-time collaborative decision-making. In addition, one study [34] innovatively introduced brain-computer interfaces into air-ground swarm control, enabling dynamic mapping between human intentions and UAV behaviors. Finally, a few works investigate finegrained collaboration among UAVs, vehicles, and humans. Miller et al.[37] designed an LLM-driven air-ground collaborative system based on the efficient reasoning ability of LLMs. It dynamically adjusts task priorities through natural language interaction between UAVs, UGVs, and humans. In terms of data collection, Han et al.[14] explored a collaborative path planning method involving UAVs, vehicles, and human groups to achieve fine-grained coordination in post-disaster response scenarios.

2.4 Issues of Existing Research

The heterogeneous multi-agent collaboration model that rely on spatial division or task-phase division generally exhibit limited coordination. The former typically assigns agents to different spatial regions based on their mobility capabilities, while the latter often decomposes a large task into sequential subtasks executed by different agents. Fine-grained collaboration better utilizes the strengths of each agent type and enables complementary cooperation. However, reasoning capabilities of LLMs are limited for highly complex tasks. Learning-based methods need large training datasets, which are hard to collect in disaster scenarios. Moreover, learning models are sensitive to agent coupling. Changes in agent numbers or status can significantly affect performance [23]. Therefore, further research is needed on collaborative scheduling of time-dependent UAVs, vehicles, and workers in disaster sensing.

Problem Formulation

In this section, we define the basic concepts, analyze the constraints of the studied problem, and present the optimization objective.

Definition 1. UAV set $UAV = \{u_0, \dots, u_i, \dots\}$, where $u_i = \langle uLoc_i, uRge_i, Fullpower_i, uPow_i, U_uptime_i, uPow_i, U_uptime_i, uPow_i, uPow_i,$ $U_{\underline{i}}$ denotes the *i*-th UAV in UAV. $uLoc_i$ represents the current location of u_i ; $uRge_i$ denotes the moving speed of u_i ; Fullpower, is the maximum distance u_i can move with full power; $uPow_i \in [0, Fullpower_i]$ indicates the current movable distance of u_i ; U_uptime_i and $U_udowntime_i$ represent the online and offline times of u_i , modeling its time-dependent behavior. UAVs refer to unmanned aerial vehicles collected from the disaster scenario that are capable of performing sensing tasks.

Definition 2. Worker set $Worker = \{w_0, \ldots, w_j, \ldots\}$, where $w_j = \langle wLoc_j, wRge_j, W_uptime_j, W_downtime_j \rangle$ denotes the j-th worker in Worker. $wLoc_i$ is the current location of w_i ; $wRge_i$ denotes the moving speed of w_i ; W_uptime_i and $W_downtime_i$ represent the online and offline times of w_i , modeling its time-dependent behavior. Workers are personnel in the disaster scenario who are skilled in UAV operation and collaboratively control UAVs to complete sensing tasks.

Definition 3. Vehicle set $Vehicle = \{v_0, \dots, v_k, \dots\}$, where $v_k = \langle vLoc_k, vRge_k, V_chargePow_k, V_uptime_k, vRge_k, v$ $V_{downtime_k}$ denotes the k-th vehicle in Vehicle. $vLoc_k$ is the current location of v_k ; $vRge_k$ denotes the moving speed of v_k ; $V_chargePow_k$ represents the charging power provided to UAVs per unit time; V_uptime_k and $V_{\underline{a}}$ downtime_k indicate the online and offline times of v_k , modeling its time-dependent behavior. Vehicles refer to electric vehicles collected from the disaster scenario that can provide charging for UAVs. The drivers can manually connect UAVs to the power supply based on the electric vehicles' energy resources.

Definition 4. Sensing task set $Task = \{task_0, \ldots, task_x, \ldots\}$, where $task_x = \langle tLoc_x, T_costPow_x \rangle$ denotes the x-th task in Task. $tLoc_x$ represents the location of $task_x$; $T_costPow_x$ is the distance that a UAV needs to move in order to complete $task_x$. Tasks are locations in the disaster scenario where workers, leveraging their proficiency in precisely maneuvering UAVs, operate them to complete sensing tasks.

Definition 5. Charging point set $Charge = \{ \operatorname{charge}_0, \ldots, \operatorname{charge}_y, \ldots \}$, where $\operatorname{charge}_y = \langle \operatorname{chLoc}_y \rangle$ denotes the y-th charging point in $Charge. \operatorname{chLoc}_y$ represents the location of charge_y . Charging points are open areas in the disaster scenario where UAVs can be recharged by vehicles under stationary and safe operation conditions. When UAVs and vehicles meet at a charging point, the driver can assist in connecting the UAVs to recharge.

Before defining the problem of this paper, we need to introduce the following constraints.

(1) When UAV u_i and worker w_j meet at location $tLoc_x$, the task task_x can be completed, and $uPow_i$ decreases by T $costPow_x$:

$$task_x = \emptyset \& uPow_i = uPow_i - T_costPow_x, \text{ if } uLoc_i = wLoc_j = tLoc_x \tag{1}$$

- (2) When u_i and w_j perform task task_x, the time consumed by both of them is $T_costPow_x/uRge_i$.
- (3) When u_i and v_k meet at charging point charge u_i , v_k can charge u_i until it is fully charged:

$$uPow_i = Fullpower_i$$
, if $uLoc_i = vLoc_k = chLoc_y$ (2)

- (4) When v_k charges u_i at charge v_k , the time cost for both is $(Fullpower_i uPow_i)/V_chargePow_k$. Note: If multiple UAVs need to be charged, v_k follows a first-come-first-served principle.
- (5) When u_i chooses charging point charge u_i , it must ensure:

$$Dis(chLoc_{y}, uLoc_{i}) \le uPow_{i} \tag{3}$$

(6) When u_i selects to execute task_x, it must ensure:

$$Dis(uLoc_i, tLoc_x) + T_costPow_x + Dis(tLoc_x, Opt_charge_u) \le uPow_i, Opt_charge_u \in Charge$$
 (4)

Problem 1 (Collaborative Scheduling of Time-dependent UAVs, Vehicles and Workers for Crowdsensing in Disaster Response): Given UAV set UAV, Worker set Worker, Vehicle set Vehicle, Task set Task, and Charging point set Charge, determine the scheduling actions $\{A_u_i^{t \times Interval}\}, \{A_w_j^{t \times Interval}\}, \{A_v_k^{t \times Interval}\}$ for $t=0,1,2,\ldots$ and $t \times Interval \in [0, LimitTime]$, so as to maximize the number of completed sensing tasks $Cplt_Tasks$:

We prove in Appendix A that the **Problem 1** is NP-hard.

4 Methodology

To solve **Problem 1**,we transform **Problem 1** into the MWIS problem on an undirected graph G = (Nd, Eg). Here, each node $nd \in Nd$ represents a weighted, feasible multi-agent collaborative action. For any two nodes nd_m , $nd_n \in Nd$, an edge $(nd_m, nd_n) \in Eg$ is established if their corresponding scheduling behaviors conflict. An independent set $S \subseteq Nd$ in graph G implies that for any nd'_m , $nd'_n \in S$, $(nd'_m, nd'_n) \notin Eg$, which, by our edge definition, means their corresponding scheduling behaviors do not conflict. Therefore, an independent set directly represents a set of feasible and non-conflicting actions for **Problem 1**. This paper sets node weights as the expected benefit per time interval of scheduling behaviors, which is positively correlated with the optimization objective of **Problem 1**. Identifying the maximum weighted independent set S^* (the independent set with the largest sum of node weights) then directly ensures the selection of the most beneficial set of compatible actions, thereby maximizing the overall mission objective. Based on this weighted undirected graph G, we propose a heterogeneous multi-agent online collaborative scheduling algorithm based on weighted undirected graph

modeling and maximum weight independent set solution, named HoCs-MPO. Its framework, as shown in Fig. 2, consists of two main modules: weighted undirected graph construction and maximum weight independent set solution. (1) Weighted undirected graph construction involves three parts: weighted undirected graph node construction, graph node weight evaluation and quantification, and weighted undirected graph generation. (2) Maximum weight independent set solution includes two parts: Heterogeneous multi-agent online collaborative scheduling algorithm based on iterated local search for maximum weight independent set (HoCs-ILS) and solution process acceleration based on multi-priority queues.

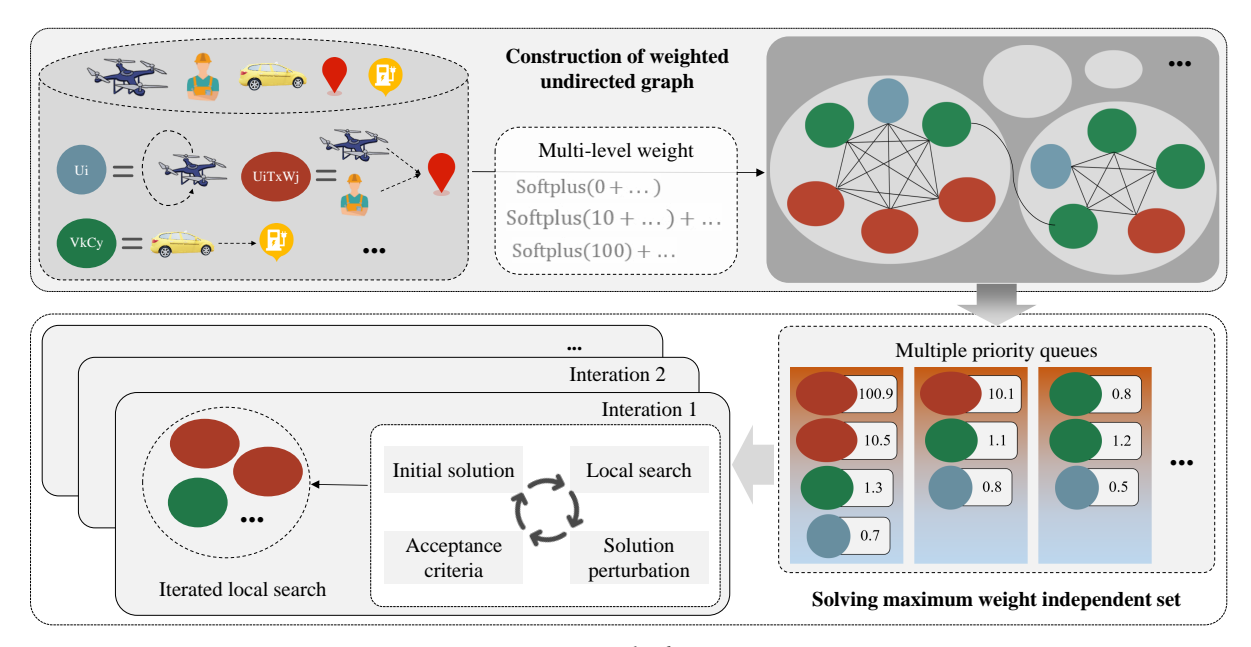


Fig. 2. Framework of HoCs-MPQ.

Weighted Undirected Graph Construction

- Weighted Undirected Graph Node Construction. To construct a weighted undirected graph, we need to first clarify its node set Nd. Collaborative scheduling of time-dependent UAVs, vehicles, and workers can result in 9 possible scenarios, meaning the set *Nd* should include 9 types of graph nodes, as shown in Fig. 3.
 - $Ui = (u_i, uLoc_i)$ represents UAV u_i staying at its current location without movement.
 - $Wj = (w_i, wLoc_i)$ represents worker w_i staying at its current location without movement.
 - $Vk = (v_k, vLoc_k)$ represents vehicle v_k staying at its current location without movement.
 - $UiTx = (u_i, tLoc_x)$ represents UAV u_i moving to the location $tLoc_x$ of task task_x.
 - $WjTx = (w_i, tLoc_x)$ represents worker w_i moving to the location $tLoc_x$ of task task_x.
 - $UiCy = (u_i, chLoc_y)$ represents UAV u_i moving to the location $chLoc_y$ of charging point charge u.
 - $VkCy = (v_k, chLoc_y)$ represents vehicle v_k moving to the location $chLoc_y$ of charging point charge v_k
 - $UiTxWj = (u_i, tLoc_x, w_i)$ represents both UAV u_i and worker w_i moving to the location $tLoc_x$ of task
 - $UiCyVk = (u_i, chLoc_u, v_k)$ represents both UAV u_i and vehicle v_k moving to the location $chLoc_u$ of charging point charge,,.

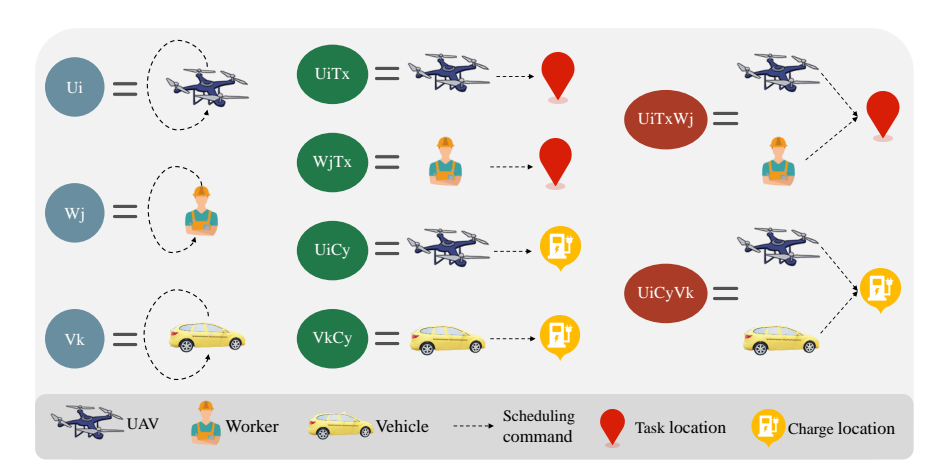


Fig. 3. Types of weighted undirected graph nodes.

Graph Node Weight Evaluation and Quantification. To construct a weighted undirected graph, we need to assign appropriate weights to the above 9 types of graph nodes. The results of these nodes can be classified into three levels: (1) $UiTxWj = (u_i, tLoc_x, w_i)$ leads to the completion of task task_x and has potential impact on the subsequent scheduling of u_i and w_i ; (2) $UiCyVk = (u_i, chLoc_u, v_k)$ leads to UAV u_i being fully charged by vehicle v_k and has potential impact on the subsequent scheduling of u_i and v_k ; (3) The other 7 types of nodes besides *UiTxW j* and *UiCyVk* only have potential impact on the subsequent scheduling of agents such as UAV u_i , worker w_i , and vehicle v_k . Therefore, we implement a hierarchical weight evaluation and quantification for these nodes. It is crucial to ensure that the quantified weights at different levels exhibit distinct orders of magnitude, thereby effectively differentiating between nodes of varying importance. Given that the optimization objective of **Problem 1** is to maximize the number of completed tasks, we assign a foundational weight of 100 to UiTxW j nodes. Furthermore, recognizing the positive impact of enhanced UAV endurance on subsequent task performance, we set the foundational weight for *UiCyVk* nodes to 10. Consequently, the remaining seven node types, excluding UiTxWj and UiCyVk, are assigned a foundational weight of 0. Building upon these foundational weight assignments, our next step involves evaluating the potential impact of individual nodes to precisely quantify their overall weights within the graph. We define the benefit derived from this potential impact as the reduction rate in the expected matching time for the agents involved. First, we need to evaluate the correlation E tL_i between the power of UAV u_i and its task execution.

$$E_{tL_i} = \frac{\left(1 - e^{-(uPow_i/\text{FullPower}_i)}\right)}{\left(1 - e^{-1}\right)}, u_i \text{ s.t. constraints (6)}$$

E_tL_i should satisfy the following properties:

- (1) The larger $uPow_i/FullPower_i$ is, the larger E_tL_i is, indicating that the more power UAV u_i has, the higher the possibility of executing tasks.
- (2) As $uPow_i$ /FullPower_i decreases, the rate of decrease in E_tL_i increases, indicating that the lower the power of UAV u_i , the greater the urgency for charging, and the possibility of executing tasks should decrease at an accelerated rate.

Let $f(uPow_i/\text{FullPower}_i) = \text{E_tL}_i, uPow_i/\text{FullPower}_i \in [0, 1]$, then

$$f'(uPow_i/\text{FullPower}_i) = \frac{e^{-(uPow_i/\text{FullPower}_i)}}{1 - e^{-1}}$$
(7)

For any $uPow_i/\text{FullPower}_i \in [0, 1]$, $e^{-(uPow_i/\text{FullPower}_i)} > 0$, i.e., $f'(uPow_i/\text{FullPower}_i) > 0$, so $f(uPow_i/\text{FullPower}_i)$ is strictly monotonically increasing on [0, 1], satisfying property (1).

$$f''(uPow_i/\text{FullPower}_i) = -\frac{e^{-(uPow_i/\text{FullPower}_i)}}{1 - e^{-1}}$$
(8)

For any $uPow_i/\text{FullPower}_i \in [0, 1]$, $-e^{-(uPow_i/\text{FullPower}_i)} < 0$, i.e., $f''(uPow_i/\text{FullPower}_i) < 0$. This means that as $uPow_i/\text{FullPower}_i$ approaches 0, $f'(uPow_i/\text{FullPower}_i)$ becomes larger, and $f(uPow_i/\text{FullPower}_i)$ decreases faster, satisfying property (2).

Next, we need to evaluate the correlation E_chL_i between the power of UAV u_i and its charging needs. E_chL_i should be negatively correlated with E_tL_i : (1) The higher the charging urgency of UAV u_i , the lower the possibility of executing tasks; (2) The faster the charging urgency of UAV u_i increases, the faster the possibility of executing tasks decreases.

$$E_chL_i = \frac{\left(1 - e^{-(1 - uPow_i/\text{FullPower}_i)}\right)}{\left(1 - e^{-1}\right)}, u_i \text{ s.t. constraints (5)}$$
(9)

The expected cost for a task $task_x$ to be matched by a UAV is as follows:

$$Du_{t}L_{x} = \frac{1}{|UAV|} \sum_{u_{i} \in UAV} \frac{ceil(Dis(uLoc_{i}, tLoc_{x})/uRge_{i}, Interval)}{E_{t}L_{i}}, u_{i} \text{ s.t. constraints (6)}$$
(10)

where Dis() represents the distance calculation function; ceil() represents the ceiling function.

Since workers do not need to be charged, the expected cost for a task $task_x$ to be matched by a worker is as follows:

$$Dw_{t}L_{x} = \frac{1}{|Worker|} \sum_{w_{i} \in Worker} ceil(\frac{Dis(wLoc_{j}, tLoc_{x})}{wRge_{j}}, Interval)$$
(11)

The expected cost for a charging point $chLoc_y$ to be matched by a UAV is as follows:

$$Du_chL_y = \frac{1}{|UAV|} \sum_{u_i \in UAV} \frac{ceil(Dis(uLoc_i, chLoc_y)/uRge_i, Interval)}{E_chL_i}, u_i \text{ s.t. constraints (5)}$$
 (12)

Since vehicles do not need to be charged, the expected cost for a charging point $chLoc_y$ to be matched by a vehicle is as follows:

$$Dv_chL_y = \frac{1}{|Vehicle|} \sum_{v_k \in Vehicle} ceil(\frac{Dis(vLoc_k, chLoc_y)}{vRge_k}, Interval)$$
(13)

The greater the expected time for worker w_j to move to task location $tLoc_x$, the lower should be the possibility of choosing task task_x. Therefore, the probabilities for worker w_j at location $wLoc_j$ to choose different tasks are as follows:

$$\{..., pw_x, ...\} = \operatorname{softmax}(..., -ceil(\frac{Dis(wLoc_j, tLoc_x)}{wRge_j}, Interval), ...)$$
 (14)

where softmax() is the normalized exponential function [2, 3].

The expected benefit per time interval for worker w_j moving from location $wLoc_j$ to a new location $wLoc_j'$ is as follows:

$$icmWj = \frac{\text{Softplus}\left(\left(\sum_{x}(\text{pw}_{x} \cdot \text{Du_tL}_{x}) - \sum_{x}(\text{pw}_{x}' \cdot \text{Du_tL}_{x})\right) / \sum_{x}(\text{pw}_{x} \cdot \text{Du_tL}_{x})\right)}{ceil(Dis(wLoc_{j}, wLoc_{j}') / wRge_{j}, Interval)}$$
(15)

where Softplus() is a smoothed version of the rectified linear unit function [9], and its purpose is to avoid negative expected benefits per time interval.

The greater the expected time for UAV u_i to move to task location $tLoc_x$, the lower should be the possibility of choosing task task_x. Therefore, the probabilities for UAV u_i at location $uLoc_i$ to choose different tasks are as follows:

$$\{..., pu_x, ...\} = \operatorname{softmax}(..., -ceil(\frac{Dis(uLoc_i, tLoc_x)}{uRge_i}, Interval), ...)$$
 (16)

The expected benefit per time interval for UAV u_i moving from location $uLoc_i$ to a new location $uLoc_i'$ is as follows:

$$icmUiT = \frac{Softplus\left(\left(\sum_{x}(pu_{x} \cdot Dw_{-}tL_{x}) - \sum_{x}(pu_{x}' \cdot Dw_{-}tL_{x})\right)/\sum_{x}(pu_{x} \cdot Dw_{-}tL_{x})\right)}{ceil(Dis(uLoc_{i}, uLoc_{i}')/uRge_{i}, Interval)}$$
(17)

The greater the expected time for UAV u_i to move to charging point $chLoc_y$, the lower should be the possibility of choosing charging point charge $_y$. Therefore, the probabilities for UAV u_i at location $uLoc_i$ to choose different charging points are as follows:

$$\{..., pu_y, ...\} = \operatorname{softmax}(..., -ceil(\frac{Dis(uLoc_i, chLoc_y)}{uRqe_i}, Interval), ...)$$
 (18)

The expected benefit per time interval for UAV u_i moving from $uLoc_i$ to a new location $uLoc_i'$ is as follows:

$$icmUiC = \frac{Softplus\left((\sum_{y}(pu_{y}\cdot Dv_chL_{y}) - \sum_{y}(pu'_{y}\cdot Dv_chL_{y}))/\sum_{y}(pu_{y}\cdot Dv_chL_{y})\right)}{ceil(Dis(uLoc_{i},uLoc'_{i})/uRge_{i},Interval)}$$
 (19)

Therefore, the comprehensive expected benefit per time interval for UAV is:

$$icmUi = \frac{uPow'_i}{\text{FullPower}_i} \cdot icmUiT + \frac{(\text{FullPower}_i - uPow'_i)}{\text{FullPower}_i} \cdot icmUiC$$
 (20)

The greater the expected time for vehicle v_k to move to charging point $chLoc_y$, the lower should be the possibility of choosing charging point charge y. Therefore, the probabilities for vehicle v_k at location $chLoc_y$ to choose different charging points are as follows:

$$\{..., pv_y, ...\} = softmax(..., -ceil(\frac{Dis(vLoc_k, chLoc_y)}{vRge_k}, Interval), ...)$$
 (21)

The expected benefit per time interval for vehicle v_k moving from location $chLoc_y$ to a new location $chLoc_y'$ is as follows:

$$icmVk = \frac{\text{Softplus}\left((\sum_{y}(\text{pv}_{y} \cdot \text{Du_chL}_{y}) - \sum_{y}(\text{pv}_{y}' \cdot \text{Du_chL}_{y}))/\sum_{y}(\text{pv}_{y} \cdot \text{Du_chL}_{y})\right)}{ceil(Dis(vLoc_{k}, vLoc_{k}')/vRge_{k}, Interval)} \tag{22}$$

The weight calculation process for UiTxWj is as follows

$$icmUiWj = \frac{\text{Softplus}(100)}{\max(ceilU, ceilW)} + icmWj + icmUi$$
 (23)

where $ceilU = ceil(Dis(uLoc_i, uLoc_i')/uRge_i, Interval)$; $ceilW = ceil(Dis(wLoc_j, wLoc_j')/wRge_j, Interval)$; max() represents taking the larger of two numbers.

The weight calculation process for UiCyVk is as follows:

$$icmUiVk = \frac{\text{Softplus}\left(10 + e^{(1 - uPow_i/\text{FullPower}_i)}\right)}{\max(ceilU, ceilV)} + icmVk + icmUi$$
 (24)

where $e^{(1-uPow_i/\text{FullPower}_i)}$ is used to quantify the additional benefit of increasing UAV power; $ceilV = ceil(Dis(vLoc_k, vLoc_k')/vRge_k, Interval)$.

The weight calculation process for nodes Ui/UiTx/UiCy refers to Equation (20); the weight calculation process for Wj, WjTx refers to Equation (15); the weight calculation process for Vk, VkCy refers to Equation (22).

4.1.3 Weighted Undirected Graph Generation. To construct a weighted undirected graph G = (Nd, Eg), we define its nodes and edges based on the problem's requirements. The generation process of this weighted undirected graph G is shown in **Algorithm 1**.

Algorithm 1: Weighted Undirected Graph Construction Algorithm (WUGCA)

```
Input: UAV, Worker, Vehicle, Task, Charge
Output: Graph G
 1: G \leftarrow \text{empty graph}
 2: Compute Du_tL<sub>x</sub>, Du_chL<sub>y</sub>, Du_chL<sub>y</sub>, Dv_chL<sub>y</sub>
 3: for each u_i \in UAV do
        G.Nd \leftarrow G.Nd \cup \{Ui\} \text{ with } w(Ui) = \text{softPlus}(0)
 4:
        for each task<sub>x</sub> \in Task such that u_i s.t. constraints (6) do
 5:
             G.Nd \leftarrow G.Nd \cup \{UiTx\}, w(UiTx) = icmUiTx
 6:
 7:
             for each w_i \in Worker such that u_i s.t. constraints (6) do
                 G.Nd \leftarrow G.Nd \cup \{UiTxWj\}, w(UiTxWj) = icmUiWj
 8:
             end for
 9:
        end for
10:
        for each charge u \in Charge such that u_i s.t. constraints (5) do
11:
             G.Nd \leftarrow G.Nd \cup \{UiCy\}, w(UiCy) = icmUiCy
12:
            for each v_k \in Vehicle do
13.
                 G.Nd \leftarrow G.Nd \cup \{UiCyVk\}, w(UiCyVk) = icmUiVk\}
14:
             end for
15:
        end for
16:
17: end for
18: for each w_i \in Worker do
        G.Nd \leftarrow G.Nd \cup \{Wj\} \text{ with } w(Wj) = \text{softPlus}(0)
19:
        for each task<sub>x</sub> \in Task do
20:
             G.Nd \leftarrow G.Nd \cup \{WjTx\} \text{ with } w(WjTx) = icmWj
21:
        end for
23: end for
24: for each v_k \in Vehicle do
25:
        G.Nd \leftarrow G.Nd \cup \{V_k\} \text{ with } w(V_k) = \text{softPlus}(0)
        for each charge _{u} \in Charge do
26:
             G.Nd \leftarrow G.Nd \cup \{VkCy\} \text{ with } w(VkCy) = icmVk
27:
        end for
28:
29: end for
30: if HasConflict(nd_m, nd_n) then
                                                                          ▶ Connect nodes when a resource conflict exists
        Add edge between nd_m and nd_n
32: end if
33: return G
```

Based on the above weighted undirected graph generation process, we analyze the graph structure. Assume that the current number of online UAVs, vehicles, and workers are |u|, |v|, and |w| respectively, the number of tasks is |task|, and the number of charging points is |charge|. The number of $Ui = (u_i, uLoc_i)$ is |u|; the number of $Vk = (v_k, vLoc_k)$ is |v|; in the worst case, the number of $UiTx = (u_i, tLoc_x)$ is |u| * |task|; the number of $WjTx = (w_j, tLoc_x)$ is |w| * |task|; in the worst case, the number of $UiCy = (u_i, chLoc_y)$ is |u| * |charge|; in the worst case, the number of $VkCy = (v_k, chLoc_y)$ is |v| * |charge|; the number of $UiTxWj = (u_i, tLoc_x, w_j)$ is |u| * |task| * |w|; in the worst case, the number of $UiCyVk = (u_i, chLoc_y, v_k)$ is |u| * |charge| * |v|. If the cumulative sum of the above nodes is denoted as N, then the order of magnitude of the number of nodes in graph G is $O(N^2)$. Therefore, with the linear growth of |u|, |w|, |v|, |task|, and |charge|, the node scale of graph G shows cubic polynomial growth, and the edge scale of graph G shows sixth-order polynomial growth, both of which are high-order polynomial growth.

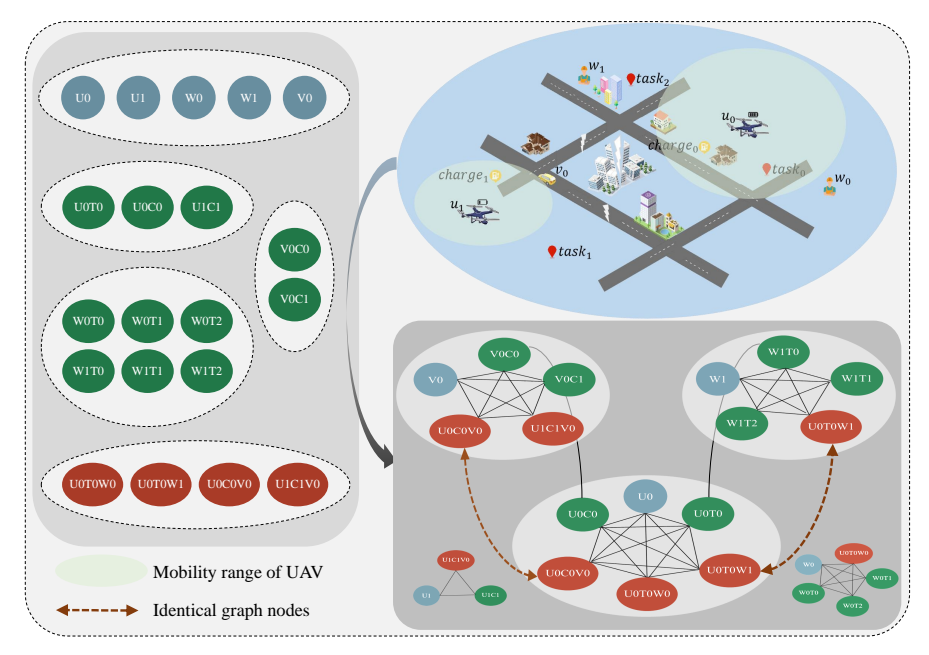


Fig. 4. Example of weighted undirected graph generation.

Fig. 4 shows an example of weighted undirected graph generation, which includes two UAVs $\{u_0, u_1\}$, two workers $\{w_0, w_1\}$, one vehicle v_0 , four tasks $\{task_0, ..., task_2\}$, and two charging points $\{charge_0, charge_1\}$. Based on constraint (6), UAVs, workers, and tasks are combined to form three-dimensional matching nodes UiTxWj; based on constraint (6), UAVs and tasks are combined to form two-dimensional matching nodes UiTx; workers and tasks are freely combined to form two-dimensional matching nodes WjTx; based on constraint (5), UAVs, vehicles, and charging points are combined to form three-dimensional matching nodes UiCyVk; based on constraint (5), UAVs and charging points are combined to form two-dimensional matching nodes UiCyVk; vehicles and charging points are freely combined to form two-dimensional matching nodes VkCy. UAVs, vehicles, and workers can remain at their original positions unchanged, forming nodes UiVy, and ViVVy respectively. Next, weights are assigned to all the above nodes based on the weighted graph node weight evaluation and quantification process (see 4.1.2). Finally, any two nodes are selected from all the above nodes, and if the scheduling behaviors corresponding to the selected nodes have conflicts, an edge connection is set between the two nodes.

4.2 Maximum Weight Independent Set Solution

The solution process of the maximum weight independent set S* of the weighted undirected graph G mainly includes two parts: (1) Due to the large scale of graph G, exact algorithms are difficult to find its maximum weight independent set S* in a short time. In order to find high-quality approximate solutions in a limited time, we design a maximum weight independent set solution algorithm based on iterative search. (2) The edges of graph G are too dense, which leads to excessive computational time overhead of the solution algorithm, making it difficult to apply to online scenarios. To reduce the computational time overhead of the algorithm, we implemented solution process acceleration based on multi-priority queues.

4.2.1 HoCs-ILS. For the weighted undirected graph constructed above, we have developed a MWIS solution algorithm based on the principles of Iterated Local Search (ILS) [32], as detailed in **Algorithm 2**. This algorithm is structured around four core modules: initial solution generation, local search, perturbation, and acceptance criterion. The initial solution is constructed using a greedy approach, leveraging a hierarchical weight-based strategy. Within the local search module, we quantify the potential value of nodes and maintain an evaluation queue to expedite the discovery of local optimal solutions. Pertaining to the perturbation strategy, our algorithm adaptively adjusts its intensity based on the quality of the current local optimal solution, thereby expanding the solution search space. Finally, the acceptance criterion module facilitates the acceptance of suboptimal solutions, enhancing the diversity of explored local solutions. Guided by this acceptance criterion, the algorithm progressively refines the final solution through a continuous cycle of local search and adaptive perturbation, until either the maximum number of iterations is reached or a predefined termination condition is satisfied.

The local search process is shown in **Algorithm 3**. We introduce a node evaluation function $\sigma(nd_m)$ to quantify the improvement value of vertex nd_m to the current solution:

$$\sigma(nd_m) = w(nd_m) - \sum_{nd_n \in N(nd_m) \cap S} w(nd_n)$$
(25)

where $w(nd_m)$ is the weight of vertex nd_m , $N(nd_m)$ is the set of neighbors of nd_m , and S is the current solution, i.e., the independent set. When $\sigma(nd_m) > 0$, including nd_m into the current solution S can bring positive benefits. The algorithm maintains a candidate queue Q and continuously outputs vertices that satisfy $\sigma(nd_m) > 0$ from Q.

Generally, local search should not undo perturbation, otherwise it would affect the expansion of the solution space. Based on this, we propose a weight-aware structural perturbation strategy, as shown in **Algorithm 4**. First, since the graph node weights are quantified at different levels (see 4.1.2), the weight hierarchical distribution characteristics are significant, which provides the implementation basis for structural perturbation. We define the function $L(nd_m)$ to assign weight levels to nodes in the graph according to their types:

$$L(nd_m) = \begin{cases} 2, & nd_m = UiTxWj\\ 1, & nd_m = UiCyVk\\ 0, & nd_m = \text{Other} \end{cases}$$
 (26)

Secondly, the core of this perturbation strategy is to create structural barriers to prevent local search from easily undoing the perturbation effect. Specifically, construct a node set R to be removed and select node nd_m from it, then construct a node set C to be added and select node nd_n from it to be added to set S, to construct structural barrier A(R, C), which specifically includes the following constraints: $nd_m \in Nd \setminus S$; $\exists nd_m \in R, (nd_n, nd_m) \in Eg$; $L(nd_m) \neq L(nd_n); \forall s \in S, (nd_n, s) \notin Eg$. The node nd_n selected based on the above constraints only conflicts with node nd_m , and does not conflict with other nodes in the current solution S, thus constructing a structural barrier.

4.2.2 Solution Process Acceleration Based on Multi-Priority Queues. The inherent density of the weighted undirected graph G poses a significant computational challenge for directly solving the MWIS problem using traditional

Algorithm 2 : HoCs-ILS

```
Input: G, maxIter
Output: S^*
 1: S \leftarrow \text{InitialSolution}(G)
 2: S \leftarrow \text{LocalSearch}(G, S)
3: S^* \leftarrow S
 4: iter, noImprovCount \leftarrow 0
 5: acceptThreshold \leftarrow 0.95
 6: while iter < maxIter do
        iter \leftarrow iter + 1
7:
        S' \leftarrow \text{Copy}(S)
 8:
        pStrength \leftarrow AdaptPerturbStrength(S, noImprovCount)
 9:
        S' \leftarrow \text{Perturbation}(G, S', pStrength)
10:
        S' \leftarrow \text{LocalSearch}(G, S')
11.
        if AcceptSolution(S, S', H, acceptThreshold) then
12:
             S \leftarrow S'
13:
             if w(S) > w(S^*) then
14:
                 S^* \leftarrow S
15:
             end if
16:
        else
17:
             noImprovCount \leftarrow noImprovCount + 1
18:
        end if
19:
        if noImprovCount > maxIter/4 then
20:
             acceptThreshold \leftarrow acceptThreshold \times 0.99
21:
        end if
23: end while
24: return S*
```

approaches like HoCs-ILS, leading to excessive time consumption. To address this, and by specifically leveraging the structural characteristics of graph G, we designed the HoCs-MPO algorithm. Its primary objective is to substantially reduce the time required to find the MWIS of the weighted undirected graph G. Specifically, HoCs-MPO builds upon the foundation of the HoCs-ILS algorithm by employing multi-priority queues to classify and store nodes associated with different agents, thereby effectively reducing the operative graph scale during the solution process. As depicted in Fig. 4, the weighted undirected graph G exhibits distinct structural characteristics:(1) Clique Structures are Prevalent: The generation process of the weighted undirected graph reveals that edges (representing conflict relationships between nodes) are triggered by shared resources among the combined elements (nodes). Consequently, all nodes that share the same element (e.g., a specific agent like worker w_0) form a clique (i.e., a complete subgraph). For instance, any task task $x \in Task$ can form a node $W0Tx = (w_0, tLocx)$ with worker w_0 . Therefore, all nodes in the set $\{W0T0, ..., W0Tx, ...\}$ conflict with each other, forming a prominent clique structure. (2) Dense within Cliques and Sparse between Cliques: The graph demonstrates a pattern of dense connections within cliques and sparse connections between cliques. Within each clique, nodes generally exhibit pervasive conflict relationships, leading to exceptionally dense edge connections. Conversely, nodes belonging to different clique structures typically share no conflict relationships, resulting in very sparse edge connections between them. Therefore, despite the overall density of the weighted undirected graph G, it possesses clearly discernible sparse regions that HoCs-MPQ exploits.

Algorithm 3 : Local Search Optimization Algorithm (LSOA)

```
Input: G, S'
Output: S''
 1: improved \leftarrow true
 2: S'' \leftarrow S'
 3: while improved do
        improved \leftarrow false
 4:
        if (nd_m \leftarrow Q.pop()) \neq nil then
 5:
             RemoveNeighbors(nd_m, S'', Eq)
                                                                        \triangleright Remove from S'' all nodes adjacent to nd_m in Eq
 6:
             S''. Add(nd_m)
 7:
             improved \leftarrow true
 8:
        end if
10: end while
11: return S"
```

Algorithm 4: Stratified Cyclic Perturbation Algorithm (SCPA)

```
Input: G, S', pStrength
Output: S
 1: S_0 \leftarrow \{nd_m \in S' | nd_m \text{ is of type Other}\}
 2: S_1 \leftarrow \{nd_m \in S' | nd_m \text{ is of type } UiCyVk\}
 3: S_2 \leftarrow \{nd_m \in S' | nd_m \text{ is of type } UiTxWj\}
 4: l \leftarrow iter \mod 3
 5: R \leftarrow \emptyset, C \leftarrow \emptyset
 6: if l = 0 and |S_0| > 0 then
         R \leftarrow \text{randomly select } min(k, |S_0|) \text{ nodes from } S_0
 8: else if l = 1 and |S_1| > 0 then
         R \leftarrow \text{randomly select } min(k, |S_1|) \text{ nodes from } S_1
10: else if l = 2 and |S_2| > 0 then
         R \leftarrow \text{randomly select } min(max(1, \lfloor k/2 \rfloor), |S_2|) \text{ nodes from } S_2
11:
13: FindDifferentLabelNeighbors(R, S', C)
                                                                              ▶ Add neighbors of R with different labels to set C
14: S \leftarrow RemoveNodesFromSolution(S', R)
                                                                                           ▶ Remove nodes in set R from solution S'
15: Shuffle(C)
16: S \leftarrow AddIndependentNodes(S, C, Eq)
                                                                                              ▶ Add nodes with no edge connection
17: return S
```

Leveraging these identified structural characteristics of graph G, we propose an incremental Maximum Weighted Independent Set solution algorithm based on multi-priority queues (HoCs-MPQ), as detailed in Algorithm 5. Initially, nodes are logically grouped based on the specific agent types they involve. Within each group, nodes are then sorted by output priority in descending order of their associated weights. A noteworthy aspect is that if a node incorporates both a UAV and other agent types, its primary grouping reference is solely the UAV category. Subsequently, nodes are dequeued from each multi-priority queue following an elastic expansion rule. As nodes are dequeued, the weighted undirected graph G' (the current working graph for the MWIS problem) is dynamically updated to reflect the newly considered nodes and their relationships. The refined subgraph G'

is then loaded into the HoCs-ILS algorithm, which computes the Maximum Weighted Independent Set for this updated subgraph. Finally, the algorithm assesses whether the Maximum Weighted Independent Set obtained in the current iteration round is superior to that from the preceding round. If no improvement is observed, the node dequeuing speed is adaptively accelerated to explore other parts of the solution space more quickly; otherwise, the dequeuing speed remains at its standard rate. There are three noteworthy points about the HoCs-MPQ algorithm:

- (1) Incremental Warm Start of the Solution (refer to line 6 of **Algorithm 5**): By gradually expanding the subgraph G', the optimal solution S^{sub} obtained from each stage is consistently utilized as the initial solution for the subsequent iteration of the HoCs-ILS algorithm. This operation serves two critical purposes: Firstly, it ensures the monotonic non-decreasing property of the solution's total weight sum, meaning that as the subgraph G' expands, the accumulated weight of the solution S^{sub} is guaranteed to gradually increase. Secondly, by initiating the HoCs-ILS algorithm from an already high-quality solution, this strategy effectively reduces ineffective exploration of the search space, thereby accelerating convergence.
- (2) High-quality Subgraph Construction: High-quality subgraphs are efficiently constructed by strategically prioritizing the output of high-weight nodes through the multi-priority queues. This operational principle primarily allows the subgraph *G'* to preferentially cover areas that are dense with high-weight nodes, ensuring that the most impactful collaborative opportunities are considered early. Furthermore, this method explicitly models the resource competition relationship between agents by prioritizing combinations that yield higher benefits, thereby guiding the solution toward more efficient resource allocation.
- (3) Elastic Expansion Rule (refer to lines 13 of Algorithm 5): Through the implementation of an exponential expansion strategy, this rule ensures that the algorithm effectively covers the dynamically constructed subgraph G' within a finite number of steps. This particular operation enables the HoCs-ILS algorithm to quickly obtain reliable approximate solutions at a low computational cost during its early stages. Subsequently, it facilitates a controlled expansion to encompass the global solution space as dictated by the problem's requirements in the later stages, striking an optimal balance between initial efficiency and comprehensive solution discovery.

As shown in Fig. 5, we have provided an intuitive description of the algorithm process of HoCs-MPQ based on the weighted undirected graph example shown in Fig. 4. This weighted undirected graph example contains two UAVs $\{u_0, u_1\}$, two workers $\{w_0, w_1\}$, one vehicle v_0 , four tasks $\{task_0, ..., task_3\}$, and two charging points $\{charge_0, charge_1\}$. First, all nodes in the example are classified according to the different agents they contain, and inserted into the corresponding queues in order of weight. Then, according to the elastic rule, nodes are output from all priority queues in sequence, and the weighted undirected graph G' to be solved is updated. Next, graph G' is loaded into the HoCs-ILS algorithm to solve the maximum weight independent set MWIS' of graph G'. Finally, it is determined whether the maximum weight independent set obtained in the current iteration round is better than that in the previous round. If not, the node dequeuing speed is accelerated, otherwise the dequeuing speed remains normal.

5 EVALUATION

5.1 Experimental Setup

5.1.1 Dataset Setup. Our proposed algorithm's performance is comprehensively evaluated using both real-world datasets and randomly simulated datasets. A summary of these datasets is presented in Table 5 in APPENDIX B. The real-world datasets include BicycleOrder data [24, 71], TaxiTrajectories data [64], and DidiOrders data [6]. The randomly simulated datasets are generated through a parameterized process, with the detailed data generation procedures available in [5].

Algorithm 5 : HoCs-MPQ

```
Input: G
Output: Sbest
 1: Initialize priority queues Q_k for each agent category k
 2: S_{best}, S_{current} \leftarrow \emptyset
 3: K \leftarrow 1
 4: while \exists Q_k \neq \emptyset and not all categories represented in solution do
        ExtractTopKNodes(K, {Q_k}, G_{sub})
                                                                                    ▶ Extract top-K nodes from each queue
 5:
        AddConflictEdges(G_{sub})
                                                                                     ▶ Add edges between conflicting nodes
 6:
 7:
        S_{candidate}, \Delta Z \leftarrow ILS(G_{sub}, S_{current})
                                                                                                        ▶ Refer to Algorithm 2
        if \Delta Z > 0 then
 8:
            S_{current} \leftarrow S_{candidate}
 9:
            if w(S_{candidate}) > w(S_{best}) then
10:
                 S_{best} \leftarrow S_{candidate}
11:
12:
             end if
        else
13:
            K \leftarrow 2K
                                                                                               ▶ Double K if no improvement
14:
        end if
15:
        RemoveNodesFromQueues(S_{current}, {Q_k})
                                                                                      ▶ Remove solution nodes from queues
16:
        CheckCategoryRepresentation(S_{current})
                                                                                       ▶ Check if every category has a node
17:
18: end while
19: return S<sub>best</sub>
```

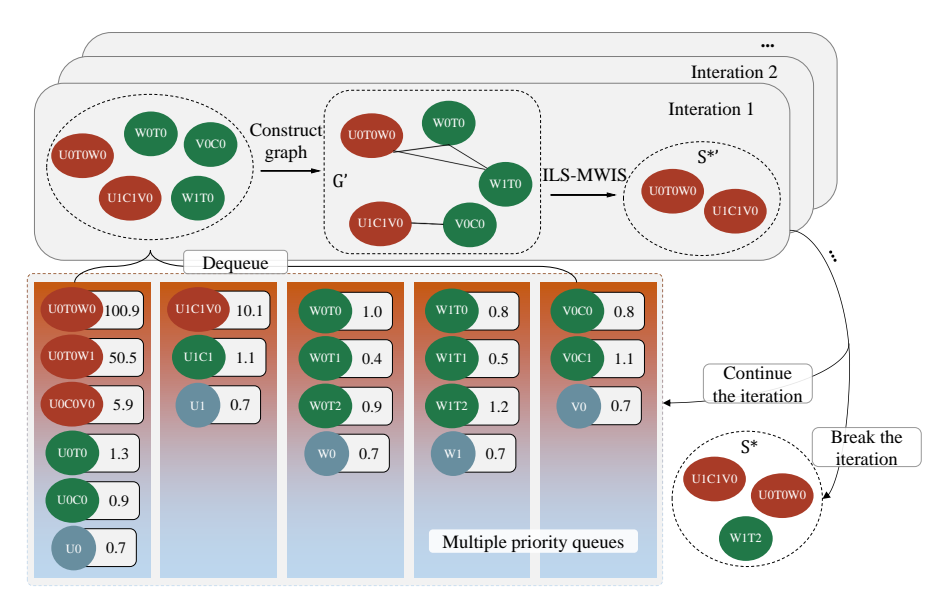


Fig. 5. Example framework diagram of the HoCs-MPQ algorithm flow.

- 5.1.2 Experiment Setup. Based on these datasets, we established five groups of experiments to comprehensively evaluate the HoCs-MPQ algorithm. These experiments investigate its performance under varying "Interval", "Limit time", "area scale, tasks number, charging point number, and agents online time", "workers number, UAVs number, and vehicles number" (representing agents number), and "task cost power and charging power". Further details regarding these experimental groups and their controlled variables can be found in Table 6 in APPENDIX B.
- 5.1.3 Comparison Algorithms. In combinatorial optimization research, solution methods are typically categorized into heuristic [22, 30, 31, 43, 55], meta-heuristic [46, 49], and training-based approaches [27, 28, 56, 63, 70]. For comparative analysis, we selected HoCs-GREEDY, HoCs-KWTA, HoCs-MADL, and HoCs-MARL as comparison algorithms. Their characteristics and implementation details are summarized in Table 7 in Appendix B;notably, HoCs-MADL and HoCs-MARL heavily reference [14]. Additionally, a comparative analysis of our proposed algorithm against several recent multi-agent deep learning algorithms, including QMIX, CW-QMIX[44], OW-QMIX, QTRAN[47], QPLEX[53], MF-QMIX[67], and SQIX [68], is presented with detailed experimental results in Appendix C. While recent efforts have explored leveraging large language models (LLMs) [25, 65] for such problems, including our own attempts[5] (detailed prompt in Appendix D), current large language models exhibit significant limitations in handling multi-constraint scheduling tasks in complex post-disaster environments, often failing to generate reasonable scheduling plans due to a lack of logical consistency and reliable reasoning.

5.2 Experimental Results

To control variables and accurately assess the impact of different factors on algorithm performance, all parameters are set to default values, except for those explicitly varied in each experimental group. The experiment is conducted in a 30×30 area scale, with 120 tasks, 20 charging points, and a 60-minute agent online time. The agents consist of 50 workers, 30 UAVs, and 20 vehicles. Each task incurs a task power cost of 3, and each vehicle has a charging power of 10. Each experiment group only changes the target variable while keeping other parameters at their default values. The following experimental results (task completion rate) are averaged over multiple experiments.

5.2.1 Experimental Results Under Different Intervals. As shown in Fig. 6, when the decision time interval increases from 5 minutes to 15 minutes, the task completion rate of the HoCs-MPQ algorithm consistently outperforms other baseline algorithms. Specifically, with a decision time interval of 5 minutes, HoCs-MPQ's average task completion rate is 83.92%, which is 55.17%, 35.65%, 18.42%, and 13.67% higher than the HoCs-GREEDY, HoCs-KWTA, HoCs-MADL, and HoCs-MARL methods, respectively. With a decision time interval of 10 minutes, HoCs-MPQ maintains a task completion rate of 75.96%, with improvements of 57.64%, 30.73%, 18.96%, and 17.96% over the baseline methods. With a decision time interval of 15 minutes, although HoCs-MPQ's average task completion rate decreases to 63.07%, it still shows improvements of 50.10%, 21.19%, 13.57%, and 13.32% compared to the baseline methods.

These results indicate that the decision time interval has a significant impact on the task completion rate, while HoCs-MPQ demonstrates significant advantages under different time constraints.

5.2.2 Experimental Results Under Different Limit Times. As shown in Fig. 7, as the duration time increases from 2 hours to 4 hours, the task completion rate of the HoCs-MPQ algorithm consistently outperforms other baseline algorithms. Specifically, with a duration time of 2 hours, HoCs-MPQ's average task completion rate is 49.16%, which is 30.97%, 24.22%, 8.91%, and 6.41% higher than the HoCs-GREEDY, HoCs-KWTA, HoCs-MADL, and HoCs-MARL methods, respectively. With a duration time of 3 hours, HoCs-MPQ's average task completion rate increases to 83.92%, with improvements of 55.17%, 35.65%, 14.17%, and 12.92% over the baseline methods. As the

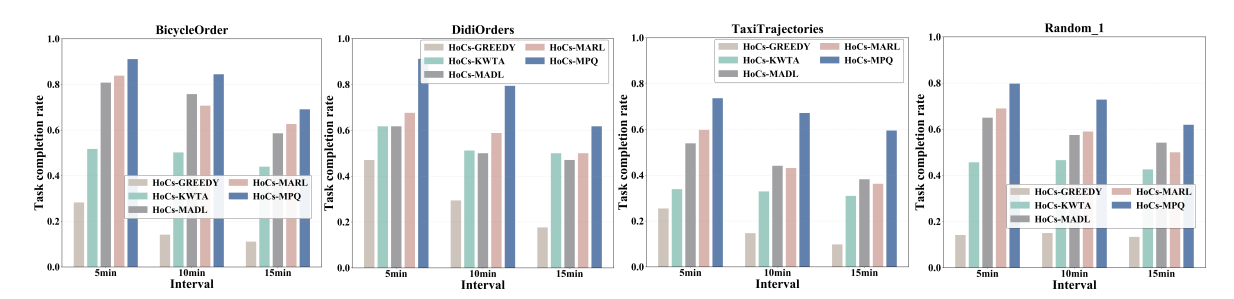


Fig. 6. Experimental results under different intervals.

duration time increases to 4 hours, HoCs-MPQ's average task completion rate further increases to 93.29%, still showing improvements of 50.71%, 18.51%, 10.79%, and 12.04% over the baseline methods.

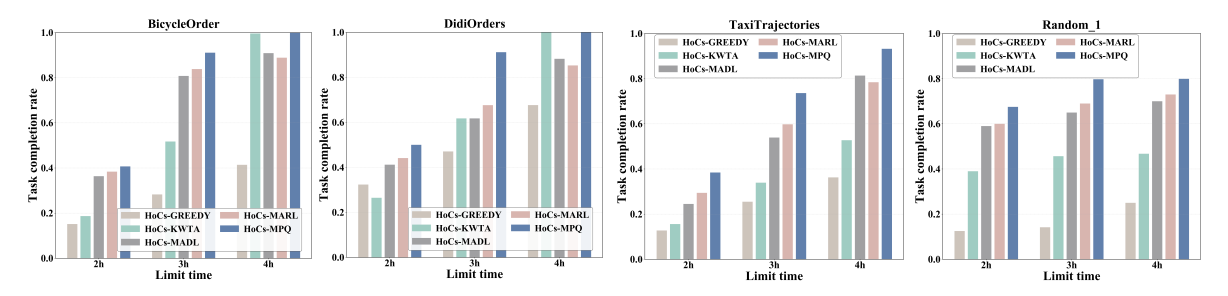


Fig. 7. Experimental results under different limit times.

These results indicates that as the duration time increases, the task completion rate of all algorithms improves, but the HoCs-MPQ algorithm maintains significant advantages under various duration time conditions, especially in performance within limited time.

Experimental Results Under Different Background Factors. As shown in Fig. 8, under different conditions of area scale, number of tasks, number of charging points, and agent online duration, the HoCs-MPQ algorithm demonstrates significant advantages. In the area scale experiment, HoCs-MPO's average task completion rate is 74.72%, which is 62.22%, 26.91%, 13.05%, and 10.72% higher than the HoCs-GREEDY, HoCs-KWTA, HoCs-MADL, and HoCs-MARL methods, respectively. In the task quantity experiment, HoCs-MPQ's average task completion rate is 70.09%, with improvements of 54.66%, 26.11%, 6.76%, and 5.76% over the baseline methods. In the charging point quantity experiment, HoCs-MPQ's average task completion rate reaches 75.11%, with improvements of 59.56%, 27.78%, 17.44%, and 14.78% over the baseline methods. In the agent online duration experiment, HoCs-MPQ's average task completion rate is 72.78%, with improvements of 56.67%, 22.56%, 13.11%, and 13.11% over the baseline methods.

These results indicate that the HoCs-MPQ algorithm can maintain stable high performance under various environmental factor changes, with the most outstanding performance in the area scale and charging point quantity experiments.

5.2.4 Experimental Results Under Different Agent Configurations. As shown in Fig. 9, the HoCs-MPQ algorithm demonstrates significant advantages under different agent quantity configurations. In the total agent quantity experiment, HoCs-MPQ's average task completion rate is 69.19%, which is 56.41%, 23.52%, 13.86%, and 11.19% higher than the HoCs-GREEDY, HoCs-KWTA, HoCs-MADL, and HoCs-MARL methods, respectively. In the worker quantity experiment, HoCs-MPQ's average task completion rate is 70.08%, with improvements of 57.03%,

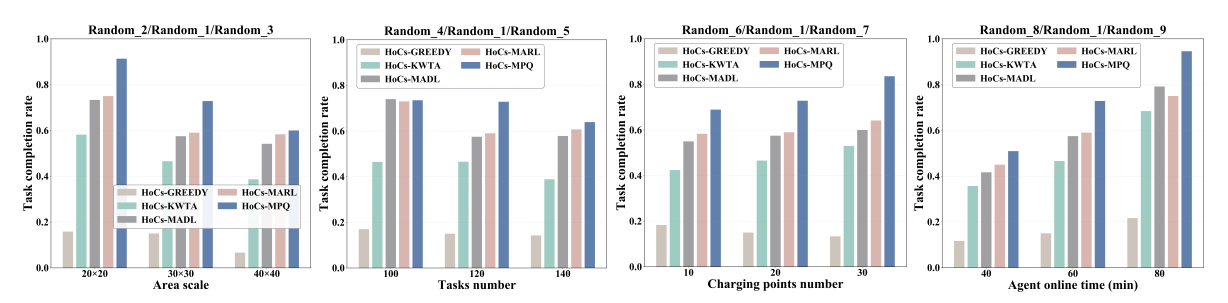


Fig. 8. Experimental results under different background factors.

28.03%, 12.75%, and 12.75% over the baseline methods. In the UAV quantity experiment, HoCs-MPQ's average task completion rate is 74.08%, with improvements of 57.14%, 27.41%, 16.41%, and 15.41% over the baseline methods. In the vehicle quantity experiment, HoCs-MPQ's average task completion rate is 71.94%, with improvements of 56.11%, 27.27%, 12.27%, and 12.27% over the baseline methods.

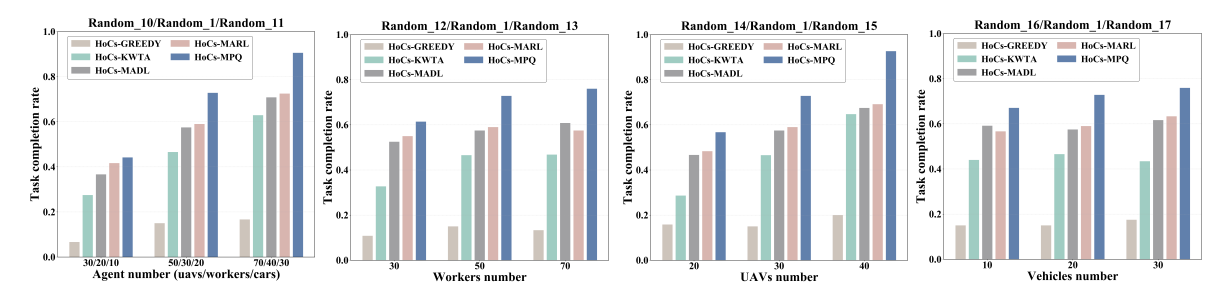


Fig. 9. Experimental results under different agent configurations.

These results indicate that the HoCs-MPQ algorithm can maintain stable high performance under various agent configurations and has strong adaptability to changes in the number of different types of agents.

5.2.5 Experimental Results Under Different Power Factors. As shown in Fig. 10, the HoCs-MPQ algorithm demonstrates significant advantages under different task power consumption and charging power conditions. In the task power consumption experiment, HoCs-MPQ's average task completion rate is 71.71%, which is 56.15%, 26.64%, 14.54%, and 13.88% higher than the HoCs-GREEDY, HoCs-KWTA, HoCs-MADL, and HoCs-MARL methods, respectively. In the charging power experiment, HoCs-MPQ's average task completion rate is 71.75%, with improvements of 55.08%, 25.74%, 15.75%, and 15.58% over the baseline methods.

These results indicate that the HoCs-MPQ algorithm has strong adaptability to changes in energy-related parameters, especially showing extremely significant advantages compared to the HoCs-GREEDY algorithm, while maintaining stable performance when facing high power consumption tasks.

5.3 Analysis and Discussion

5.3.1 Simulation Trajectory Analysis of Multiple Agents. We constructed a 3D urban ruins scenario using the Unity engine[50], in which the initial positions of 10 unmanned aerial vehicles (UAVs), 10 vehicles, and 15 workers were configured. The collaborative scheduling of these heterogeneous agents was carried out based on the proposed algorithm HoAs-MPQ. As shown in Fig. 11a, simulation results show that the trajectories of the UAVs, vehicles, and workers exhibit significant spatial and temporal overlap, indicating a high level of interaction and coordination. These findings suggest that HoAs-MPQ effectively facilitates collaborative behavior among the

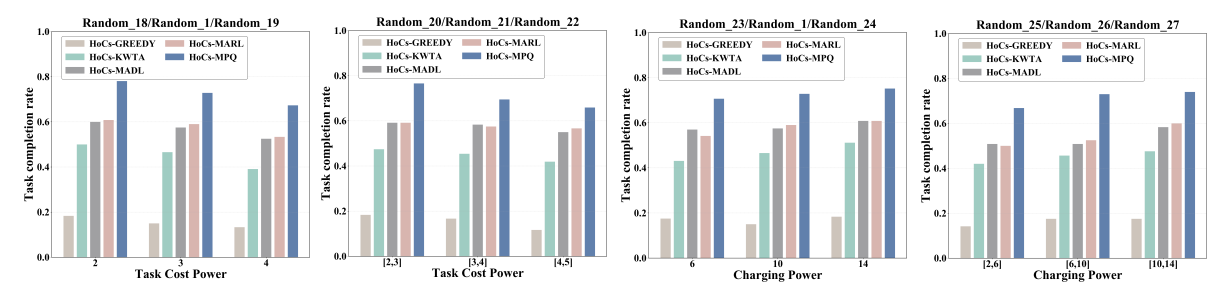


Fig. 10. Experimental results under different power factors.

agents, thereby improving task efficiency and overall system performance. Furthermore, constrained by venue availability, policy regulations, and equipment limitations, we conducted a small-scale, restricted real-world scenario validation. As illustrated in Fig. 11b, our experimental setup comprised a single UAV, a three-cell UAV battery pack, a mobile phone, and a UAV control handle. During the field test conducted at Xi'an Kunming Pool Qixi Park, the UAV successfully captured photographs of three different buildings, namely a large commemorative statue, an unfinished building, and an aquatic landscape, at 9:22, 9:48, and 9:57, with a battery replacement performed at 9:40. These real-world experiments demonstrate the practical applicability and operational viability of our proposed algorithm in authentic scenarios.



(a) Multi-agent coordination in 3D disaster scenarios. (b) Real-world experiment. Fig. 11. Overview of simulation and real-world experiment scenarios.

5.3.2 Comparison Between HoCs-ILS and HoCs-MPQ Methods. As shown in Table 1, The experimental results show that HoCs-MPQ significantly improves computational efficiency on large-scale graph structures, with the advantage becoming more apparent as the number of nodes increases. On the TaxiTrajectories dataset, the decision time is reduced by 98.7%, and on the Random_1 dataset, it is reduced by 99.7%. On the small-scale DidiOrders dataset, the two algorithms perform similarly, confirming that our algorithm's performance advantage positively correlates with the graph scale. The above experimental data fully demonstrates that the HoCs-MPQ algorithm exhibits excellent performance and time efficiency on various real-world scenarios and randomly generated datasets. As the scenario scale and problem complexity increase, the advantages of HoCs-MPQ become more apparent. While maintaining similar solution quality, HoCs-MPQ reduces computation time from tens of seconds to less than 1 second, which has important practical value for real-time scheduling systems.

Dataset	Task com	pletion rate	Decision time (s)		
	HoCs-ILS HoCs-MPQ		HoCs-ILS	HoCs-MPQ	
TaxiTrajectories	0.6569	0.6716	38.48	0.50	
BicycleOrder	0.8586	0.8444	32.23	0.58	
DidiOrders	0.8529	0.7941	0.10	0.10	
Random_1	0.7250	0.7283	56.38	0.18	

Table 1. Comparison between HoCs-ILS and HoCs-MPQ methods.

5.3.3 Comparison Between Hierarchical Weights and Uniform Weights. For the uniform weight experiment, Equation (23) was mainly modified to:

$$icmUiWj = \frac{\text{Softplus}(1)}{max(ceilU, ceilW)} + icmWj + icmUi$$
 (27)

And Equation (24) was modified to:

$$icmUiVk = \frac{\text{Softplus}\left(\left(e^{(1-uPow_i/\text{FullPower}_i)}\right)/e\right)}{max(ceilU,ceilV)} + icmVk + icmUi \tag{28}$$

As shown in Table 2, the hierarchical weight scheme outperforms the uniform weight scheme mainly for the following reasons: (1) Clear distinction of decision priorities: Hierarchical weights assign clear priorities to different types of nodes through order-of-magnitude differences, allowing the algorithm to first focus on task completion, then consider energy replenishment, and finally consider potential benefits from operations. This hierarchical design directly corresponds to the optimization objective (maximizing task completion), while uniform weights cannot effectively distinguish node importance. (2) Optimization of resource allocation strategies: The hierarchical weight mechanism enables the algorithm to make more reasonable decisions when resources are limited. The experimental results show that on the BicycleOrder dataset, the task completion rate of the hierarchical weight scheme is 39.15% higher than that of the uniform weight scheme, indicating that clear priority division can significantly improve system performance in complex scenarios. (3) Consideration of long-term decision benefits: Hierarchical weights not only focus on immediate returns but also guide the algorithm to make decisions beneficial for long-term optimization objectives through weight design. For example, setting moderate weights for UAV charging nodes ensures the necessity of energy replenishment while avoiding the loss of task execution opportunities due to excessive charging. (4) Adaptability to problem characteristics: The hierarchical weight scheme is designed according to the optimization objective of Problem 1, assigning the highest weight to task completion nodes, fully reflecting the core focus of the problem, while the uniform weight scheme lacks this problem-specific adaptation.

Table 2. Comparison of task completion rate between HoCs-MPQ with uniform weights and hierarchical weights.

Dataset	BicycleOrder	DidiOrders	TaxiTrajectories	Random_1
HoCs-MPQ (Uniform)	0.4529	0.7353	0.5707	0.5042
HoCs-MPQ (Hierarchical)	0.8444	0.7941	0.6716	0.7283

Hierarchical weight design enables the scheduling algorithm to clearly distinguish the contributions of different node types to the overall scheduling objective, allowing the system to prioritize nodes that directly promote task completion, thus ensuring efficiency and rationality. As shown in Fig .12, the hierarchical weight setting results in a clear and non-overlapping distribution of the three types of node weights, further validating the critical role of hierarchical weights in improving system performance. Future work will further investigate multi-level adaptive weighting mechanisms to enhance the generalization and robustness of the algorithm in various application scenarios.

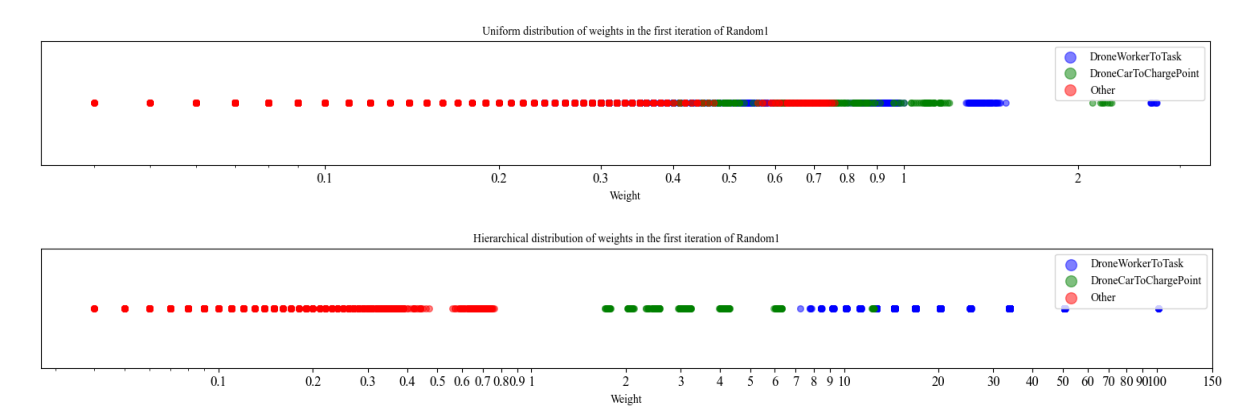


Fig. 12. Distribution of weights in the first iteration of Random1.

5.3.4 Analysis of settings close to actual scenarios. To thoroughly assess the practical applicability and resilience of our algorithm, we conducted a series of experiments incorporating various stochastic elements designed to mimic real-world operational challenges. Firstly, to account for the unpredictable effects of wind resistance on UAV operations, the energy consumed by UAVs per unit distance was randomized, drawing values from a uniform distribution within the range of [0.1, 0.4]. Secondly, considering the inevitable communication overhead in a distributed system, each scheduling decision incurred an additional random energy cost, sampled from [0.1, 0.5]. Thirdly, to evaluate the algorithm's robustness against system failures and network unreliability, agents were subjected to sudden failures, with each agent having a probability p (between 0.01 and 0.05) of immediately going offline. Furthermore, acknowledging the potential for communication delays, data packet loss, or anomalous network fluctuations in practical scenarios, we simulated instances where successful matches could fail, with a probability ranging from 5% to 10%. The comparative outcomes under these challenging conditions are presented in Table 3. These results unequivocally demonstrate that our algorithm consistently maintains high performance even under adverse and unpredictable circumstances, thereby validating its robust design and suitability for real-world deployments.

Datasets	base	wind resistance power	communication	sudden agent	ıt packet	
		cost	power cost	failues	loss	
BicycleOrder	0.8444	0.8181	0.7878	0.7566	0.8101	
TaxiTrajectories	0.6716	0.6578	0.6559	0.5882	0.6412	
DidiOrders	0.7941	0.7618	0.7706	0.7324	0.7412	
Random 1	0.7283	0.6833	0.6750	0.7008	0.6825	

Table 3. Task completion rate under various realistic scenario settings.

5.3.5 Discussion and Analysis of Scalability in Large-Scale Graphs. To evaluate the scalability of our proposed HoCs-MPQ algorithm, we conducted experiments on distinct large-scale graph scenarios. Across the comparative experiments reported in Table 4, we isolate the distinct influences of agent count and spatial density (agent number/area scale) on HoCs-MPQ's runtime. When agent, task, and charging point counts increase simultaneously (Row 1 vs. Row 2), decision time rises sharply (0.18 s \rightarrow 673.2 s), indicating that sheer scale can render computation the principal bottleneck. With other parameters held constant (Row 2 vs. Row 3), a decrease in spatial density reduces runtime, because denser deployments generate more coverage relations and produce a denser graph.

In the large-scale probe (=1000 agents with proportionally scaled tasks, area, and charging points), holding spatial density approximately constant, a decrease in agent count reduces runtime (Row 4 vs. Row 5). Conversely, when both agent count and spatial density decrease (Row 4 vs. Row 6), the runtime also decreases, suggesting that sparser deployments with fewer agents lead to reduced graph complexity and lower computational cost. Collectively, these results demonstrate that runtime is jointly determined by agent count and spatial density via their effect on graph sparsity and the number of coverage-dependent node combinations.

Area	Tasks	Charging point	Agent number	Spatial density	Task completion	Decision
scale	number	number			rate	time (s)
30×30	120	20	(50,30,20)	1:9	0.9111	0.18
60×60	480	80	(200,120,80)	1:9	0.8313	673.2
60×60	480	80	(80,48,32)	1:22.5	0.3063	223.0
150×150	600	200	(500,300,200)	1:22.5	0.9317	433.6
90×90	600	200	(180,108,72)	1:22.5	0.4967	291.3
150×150	600	200	(300,180,120)	1:37.5	0.4700	289.1

Table 4. HoCs-MPQ performance on large-scale graph scenarios.

Collectively, the comparative experiments reported in Table 4 indicate that HoCs-MPQ's computation time is governed not merely by the total number of agents but more critically by their spatial density. The root cause is the graph-construction stage: nodes and edges are instantiated only when a UAV's remaining energy suffices to cover a task or a charging point, so the effective graph size grows with coverage-dependent combinatorial terms. In particular, the number of graph elements scales with factors such as (UAV count) × (worker count) × (tasks reachable by a fully charged UAV) or (UAV count) × (vehicle count) × (charging points reachable by a fully charged UAV), which explains the approximate cubic behavior of graph construction, i.e., $O(N^3)$, where N reflects these coverage-dependent combinations. Nevertheless, the worst-case $O(N^3)$ growth is unlikely to materialize in many practical, large-area disaster deployments: real scenarios typically exhibit relatively spatial density, substantially reducing the number of coverage relationships and thus keeping the actual graph size well below the worst-case bound. Moreover, queueing structures accelerate MWIS solving and further mitigate observed runtimes. Therefore, while we retain the theoretical caveat that initial graph construction is $O(N^3)$, both our experimental results and realistic deployment characteristics suggest that HoCs-MPQ's runtime will not necessarily scale linearly or cubically with agent count in typical sparse, large-area scenarios.

6 Conclusion and Future Work

6.1 Conclusion

Catastrophic natural disasters (such as earthquakes) are extremely destructive, and real-time, accurate sensing of the post-disaster environment situation is crucial for efficiently organizing post-disaster rescue operations. In this paper, we propose a Heterogeneous Multi-Agent Online Collaborative Scheduling Algorithm (HoCs-MPQ) for the collaborative scheduling problem of time-dependent UAVs, vehicles, and workers in post-disaster response crowd sensing.

Specifically, (1) we model the collaborative scheduling problem of UAVs, vehicles, and workers as a maximum weight independent set solution problem based on a weighted undirected graph. We capture the collaborative relationships between multiple elements through graph node design and embody the conflict relationships between multiple elements through edge connections between nodes. Then, by solving the maximum weight independent set of the weighted undirected graph, we maximize the collaboration between UAVs, workers, and vehicles to enhance sensing effects.(2) Since the weighted undirected graph constructed in this paper is a dense graph, solving its maximum weight independent set faces a huge computational burden. Under computational

resource limitations and time sensitivity constraints, we significantly accelerate the solution process by utilizing the sequential indexing characteristics of multi-priority queues based on the graph structure characteristics.

Finally, we conducted detailed experiments based on rich real data and simulated data. Compared with baseline algorithms (HoCs-GREEDY, HoCs-KWTA, HoCs-MADL, HoCs-MARL), HoCs-MPQ shows significant improvement in task completion rate, with average increases of 54.13%, 23.82%, 14.12%, and 12.89%, respectively. Additionally, the computation time for a single online scheduling decision of HoCs-MPQ does not exceed 3 seconds, effectively meeting the low latency requirements of online scenario sensing decisions.

6.2 Future Work

However, there are still several aspects of this research worth further exploration:

- (1) The weighted undirected graph constructed in this paper is a dense graph. Although we iteratively construct subgraphs through multi-priority queues to reduce its scale as much as possible, the time complexity of graph construction is still enormous. In the future, efficient weighted undirected graph construction algorithms will be the focus of our research.
- (2) Multi-priority queues mainly sort nodes based on node weights, without fully utilizing the structural information of the graph and historical search experience. This may lead to repeated exploration of similar but suboptimal regions of the solution space, affecting the convergence efficiency of the algorithm. In the future, we should focus on exploring node evaluation methods based on self-learning, better guiding the selection of high-potential nodes by analyzing historical search trajectories and structural features of excellent solutions.
- (3) To further enhance HoCs-MPQ's scalability for ultra-large-scale disaster response, future work will focus on optimizing candidate node management and search. We aim to apply Reinforcement Learning to optimize HoCs-ILS's internal search, learning to adaptively adjust parameters for faster convergence and reduced computation. Intelligent pre-filtering and pruning mechanisms will be developed to reduce the initial candidate pool for multipriority queues, significantly lightening the computational burden. Furthermore, we will refine elastic expansion rules and queue prioritization through learned policies, enabling more adaptive and efficient exploration of the solution space.

7 Acknowledgment

This work was supported in part by the National Nat ural Science Foundation of China (No. 62502364, No. 62332014), the Postdoctoral Fellowship Program (Grade C) of China Postdoctoral Science Foundation (GZC20241315), the China Postdoctoral Science Foundation (2024M762554), the Key Research and Development Projects of Shaanxi Province (No. 2024GX-YBXM-107), the Natural Science Basic Research Program of Shaanxi (2025JC-YBQN-872) and the Fundamental Research Funds for the Central Universities (ZYTS25078).

References

- [1] ADREM, SNSE, and NDRC et al. 2023. 2023 Global Natural Disaster Assessment Report. https://www.gddat.cn/gw/micro-filesimple/api/file/showFile/920804e8-0192-89fdf283-0012-ff808081. Accessed: 2025-02-28, Published: 2024-10-13.
- [2] Ludwig Boltzmann. 1868. Studien uber das gleichgewicht der lebenden kraft. Wissenschaftliche Abhandlungen 1 (1868), 49-96.
- [3] John S Bridle. 1990. Probabilistic interpretation of feedforward classification network outputs, with relationships to statistical pattern recognition. In Neurocomputing: Algorithms, architectures and applications. Springer, 227-236.
- [4] Gordon Christie, Adam Shoemaker, Kevin Kochersberger, Pratap Tokekar, Lance McLean, and Alexander Leonessa. 2016. Radiation Search Operations using Scene Understanding with Autonomous UAV and UGV. arXiv:1609.00017 [cs.RO] https://arxiv.org/abs/1609.00017
- [5] CocaColaZero. 2025. Collaborative-Scheduling-of-Time-dependent-Agent: GitHub Repository. https://github.com/CocaColaZero/ Collaborative-Scheduling-of-Time-dependent-Agent. Accessed: 2025-04-26.
- [6] DidiGAIA 2025. GAIA: Didi's Spatiotemporal Open Data Platform. https://gaia.didichuxing.com. Accessed: 2025-04-25.
- [7] Lige Ding, Dong Zhao, Mingzhe Cao, and Huadong Ma. 2021. When crowdsourcing meets unmanned vehicles: Toward cost-effective collaborative urban sensing via deep reinforcement learning. IEEE Internet of Things Journal 8, 15 (2021), 12150-12162.

- [8] DJI Enterprise. 2024. FlightHub 2 Cloud-Based Drone Operations Management Platform. https://enterprise.dji.com/cn/flighthub-2. Accessed: 2025-07-29.
- [9] Charles Dugas, Yoshua Bengio, François Bélisle, Claude Nadeau, and René Garcia. 2000. Incorporating second-order functional knowledge for better option pricing. Advances in neural information processing systems 13 (2000).
- [10] Luwei Fu, Zhiwei Zhao, Geyong Min, Wang Miao, Liang Zhao, and Wenjie Huang. 2022. Energy-efficient 3-d data collection formulti-uav assisted mobile crowdsensing. IEEE Trans. Comput. 72, 7 (2022), 2025–2038.
- [11] Payam Ghassemi, David DePauw, and Souma Chowdhury. 2019. Decentralized dynamic task allocation in swarm robotic systems for disaster response. In 2019 international symposium on multi-robot and multi-agent systems (mrs). IEEE, 83–85.
- [12] Kamal Gulati, Raja Sarath Kumar Boddu, Dhiraj Kapila, Sunil L. Bangare, Neeraj Chandnani, and G. Saravanan. 2022. A review paper on wireless sensor network techniques in Internet of Things (IoT). Materials Today: Proceedings 51 (2022), 161–165. https://doi.org/10.1016/j.matpr.2021.05.067 CMAE'21.
- [13] Bin Guo, Sicong Liu, and Zhiwen Yu. 2022. Cyber-Physical-Human Integrated Collective Intelligence Computing. China Machine Press. In Chinese.
- [14] Lei Han, Chunyu Tu, Zhiwen Yu, Zhiyong Yu, Weihua Shan, Liang Wang, and Bin Guo. 2024. Collaborative Route Planning of UAVs, Workers, and Cars for Crowdsensing in Disaster Response. IEEE/ACM Trans. Netw. 32, 4 (May 2024), 3606–3621. https://doi.org/10.1109/TNET.2024.3395493
- [15] Viviane Herdel, Lee J Yamin, and Jessica R Cauchard. 2022. Above and beyond: A scoping review of domains and applications for human-drone interaction. In *Proceedings of the 2022 CHI Conference on Human Factors in Computing Systems*. 1–22.
- [16] Yue Hu, Yifan Lu, Runsheng Xu, Weidi Xie, Siheng Chen, and Yanfeng Wang. 2023. Collaboration helps camera overtake lidar in 3d detection. In *Proceedings of the IEEE/CVF Conference on Computer Vision and Pattern Recognition*. 9243–9252.
- [17] Shariq Iqbal, Christian A Schroeder de Witt, Bei Peng, Wendelin Böhmer, Shimon Whiteson, and Fei Sha. 2020. Ai-qmix: Attention and imagination for dynamic multi-agent reinforcement learning. arXiv preprint arXiv:2006.04222 (2020).
- [18] Michail Kalaitzakis, Brennan Cain, Nikolaos Vitzilaios, Ioannis Rekleitis, and Jason Moulton. 2021. A marsupial robotic system for surveying and inspection of freshwater ecosystems. *Journal of Field Robotics* 38, 1 (2021), 121–138.
- [19] Yunchuan Kang, Houbing Herbert Song, Tian Wang, Shaobo Zhang, Mianxiong Dong, and Anfeng Liu. 2025. A trust and bundling-based task allocation scheme to enhance completion rate and data quality for mobile crowdsensing. *Computer Networks* 262 (2025), 111189. https://doi.org/10.1016/j.comnet.2025.111189
- [20] Marko Krizmancic, Barbara Arbanas, Tamara Petrovic, Frano Petric, and Stjepan Bogdan. 2020. Cooperative aerial-ground multi-robot system for automated construction tasks. *IEEE Robotics and Automation Letters* 5, 2 (2020), 798–805.
- [21] Geert-Jan M Kruijff, Ivana Kruijff-Korbayová, Shanker Keshavdas, Benoit Larochelle, Miroslav Janíček, Francis Colas, Ming Liu, Francois Pomerleau, Roland Siegwart, Mark A Neerincx, et al. 2014. Designing, developing, and deploying systems to support human–robot teams in disaster response. Advanced Robotics 28, 23 (2014), 1547–1570.
- [22] Boyang Li, Yurong Cheng, Ye Yuan, Guoren Wang, and Lei Chen. 2019. Three-Dimensional Stable Matching Problem for Spatial Crowdsourcing Platforms. In Proceedings of the 25th ACM SIGKDD International Conference on Knowledge Discovery & Data Mining, KDD 2019, Anchorage, AK, USA, August 4-8, 2019, Ankur Teredesai, Vipin Kumar, Ying Li, Rómer Rosales, Evimaria Terzi, and George Karypis (Eds.). ACM, 1643–1653. https://doi.org/10.1145/3292500.3330879
- [23] Jinna Li, Lin Yuan, Weiran Cheng, Tianyou Chai, and Frank L Lewis. 2024. Reinforcement Learning for Synchronization of Heterogeneous Multiagent Systems by Improved *Q*-Functions. *IEEE Transactions on Cybernetics* (2024).
- [24] Yexin Li, Yu Zheng, Huichu Zhang, and Lei Chen. 2015. Traffic prediction in a bike-sharing system. In *Proceedings of the 23rd SIGSPATIAL international conference on advances in geographic information systems.* 1–10.
- [25] Zhonghang Li, Lianghao Xia, Jiabin Tang, Yong Xu, Lei Shi, Long Xia, Dawei Yin, and Chao Huang. 2024. Urbangpt: Spatio-temporal large language models. In *Proceedings of the 30th ACM SIGKDD Conference on Knowledge Discovery and Data Mining*. 5351–5362.
- [26] Bo Liu, Qiang Liu, Peter Stone, Animesh Garg, Yuke Zhu, and Anima Anandkumar. 2021. Coach-player multi-agent reinforcement learning for dynamic team composition. In *International Conference on Machine Learning*. PMLR, 6860–6870.
- [27] Chi Harold Liu, Zheyu Chen, and Yufeng Zhan. 2019. Energy-efficient distributed mobile crowd sensing: A deep learning approach. *IEEE Journal on Selected Areas in Communications* 37, 6 (2019), 1262–1276.
- [28] Chi Harold Liu, Chengzhe Piao, and Jian Tang. 2020. Energy-efficient UAV crowdsensing with multiple charging stations by deep learning. In *IEEE INFOCOm 2020-IEEE conference on computer communications*. IEEE, 199–208.
- [29] Chi Harold Liu, Yinuo Zhao, Zipeng Dai, Ye Yuan, Guoren Wang, Dapeng Wu, and Kin K Leung. 2020. Curiosity-driven energy-efficient worker scheduling in vehicular crowdsourcing: A deep reinforcement learning approach. In 2020 IEEE 36th International conference on data engineering (ICDE). IEEE, 25–36.
- [30] Kexin Liu and Yinyan Zhang. 2025. Distributed Dynamic Task Allocation for Moving Target Tracking of Networked Mobile Robots Using k-WTA Network. *IEEE Trans. Neural Networks Learn. Syst.* 36, 3 (2025), 5795–5802. https://doi.org/10.1109/TNNLS.2024.3377433
- [31] Mei Liu, Yutong Li, Yingqi Chen, Yimeng Qi, and Long Jin. 2024. A Distributed Competitive and Collaborative Coordination for Multirobot Systems. IEEE Trans. Mob. Comput. 23, 12 (2024), 11436–11448. https://doi.org/10.1109/TMC.2024.3397242

- [32] Helena Ramalhinho Lourenço, Olivier C Martin, and Thomas Stützle. 2018. Iterated local search: Framework and applications. In Handbook of metaheuristics. Springer, 129-168.
- [33] Yiwen Luo, Xiaoheng Deng, Wendong Zhang, Yan Ke, Shaohua Wan, and Yurong Qian. 2024. Collaborative intelligent delivery with one truck and multiple heterogeneous drones in COVID-19 pandemic environment. IEEE Transactions on Intelligent Transportation Systems 25, 7 (2024), 7907-7920.
- [34] Hemanth Manjunatha, Joseph P Distefano, Apurv Jani, Payam Ghassemi, Souma Chowdhury, Karthik Dantu, David Doermann, and Ehsan T Esfahani. 2020. Using physiological measurements to analyze the tactical decisions in human swarm teams. In 2020 IEEE International Conference on Systems, Man, and Cybernetics (SMC). IEEE, 256-261.
- [35] David A. McEntire. 2021. Disaster Response and Recovery: Strategies and Tactics for Resilience. John Wiley & Sons.
- [36] Nathan Michael, Shaojie Shen, Kartik Mohta, Vijay Kumar, Keiji Nagatani, Yoshito Okada, Seiga Kiribayashi, Kazuki Otake, Kazuya Yoshida, Kazunori Ohno, et al. 2014. Collaborative mapping of an earthquake damaged building via ground and aerial robots. In Field and service robotics: results of the 8th international conference. Springer, 33-47.
- [37] Ian D Miller, Fernando Cladera, Trey Smith, Camillo Jose Taylor, and Vijay Kumar. 2022. Stronger together: Air-ground robotic collaboration using semantics. IEEE Robotics and Automation Letters 7, 4 (2022), 9643-9650.
- [38] Sara Minaeian, Jian Liu, and Young-Jun Son. 2015. Vision-based target detection and localization via a team of cooperative UAV and UGVs. IEEE Transactions on systems, man, and cybernetics: systems 46, 7 (2015), 1005-1016.
- [39] Syed Agha Hassnain Mohsan, Muhammad Asghar Khan, Fazal Noor, Insaf Ullah, and Mohammed H Alsharif. 2022. Towards the unmanned aerial vehicles (UAVs): A comprehensive review. Drones 6, 6 (2022), 147.
- [40] George L Nemhauser, Laurence A Wolsey, and Marshall L Fisher. 1978. An analysis of approximations for maximizing submodular set functions-I. Mathematical programming 14 (1978), 265-294.
- [41] Farzad Niroui, Kaicheng Zhang, Zendai Kashino, and Goldie Nejat. 2019. Deep reinforcement learning robot for search and rescue applications: Exploration in unknown cluttered environments. IEEE Robotics and Automation Letters 4, 2 (2019), 610-617.
- [42] Generalleutnant Hermann Plocher. 2017. The German Air Force Versus Russia, 1943. Pickle Partners Publishing.
- [43] Yimeng Qi, Long Jin, Xin Luo, Yang Shi, and Mei Liu. 2022. Robust k-WTA Network Generation, Analysis, and Applications to Multiagent Coordination. IEEE Trans. Cybern. 52, 8 (2022), 8515-8527. https://doi.org/10.1109/TCYB.2021.3079457
- [44] Tabish Rashid, Gregory Farquhar, Bei Peng, and Shimon Whiteson. 2020. Weighted QMIX: Expanding Monotonic Value Function Factorisation for Deep Multi-Agent Reinforcement Learning. In Advances in Neural Information Processing Systems, H. Larochelle, M. Ranzato, R. Hadsell, M.F. Balcan, and H. Lin (Eds.), Vol. 33. Curran Associates, Inc., 10199-10210. https://proceedings.neurips.cc/ paper_files/paper/2020/file/73a427badebe0e32caa2e1fc7530b7f3-Paper.pdf
- [45] Stuart J Russell and Peter Norvig. 2016. Artificial intelligence: a modern approach. pearson.
- [46] Rezvan Salimi, Sadoon Azizi, and Javad Dogani. 2025. A hybrid priority-aware genetic algorithm and opposition-based learning for scheduling IoT tasks in green fog computing. Comput. Networks 267 (2025), 111349. https://doi.org/10.1016/J.COMNET.2025.111349
- [47] Kyunghwan Son, Daewoo Kim, Wan Ju Kang, David Earl Hostallero, and Yung Yi. 2019. Otran: Learning to factorize with transformation for cooperative multi-agent reinforcement learning. In International conference on machine learning. PMLR, 5887-5896.
- [48] Hao Sun, Juntao Fei, Guoping Zhang, and Mande Xie. 2025. A multi-agent-based dynamic charging strategy for UAV-assisted wireless rechargeable sensor networks. Computer Networks 259 (2025), 111081. https://doi.org/10.1016/j.comnet.2025.111081
- [49] Mozhdeh Tanha, Mirsaeid Hosseini Shirvani, and Amir Masoud Rahmani. 2021. A hybrid meta-heuristic task scheduling algorithm based on genetic and thermodynamic simulated annealing algorithms in cloud computing environments. Neural Comput. Appl. 33, 24 (2021), 16951-16984. https://doi.org/10.1007/S00521-021-06289-9
- [50] Unity Technologies. 2023. Unity Game Engine. https://unity.com/.
- [51] Haoyang Wang, Xuecheng Chen, Yuhan Cheng, Chenye Wu, Fan Dang, and Xinlei Chen. 2022. H-swarmloc: Efficient scheduling for localization of heterogeneous may swarm with deep reinforcement learning. In Proceedings of the 20th ACM Conference on Embedded Networked Sensor Systems. 1148-1154.
- [52] Haoyang Wang, Jingao Xu, Chenyu Zhao, Zihong Lu, Yuhan Cheng, Xuecheng Chen, Xiao-Ping Zhang, Yunhao Liu, and Xinlei Chen. 2024. TransformLoc: Transforming MAVs into Mobile Localization Infrastructures in Heterogeneous Swarms. In IEEE INFOCOM 2024 -IEEE Conference on Computer Communications. IEEE, 1101-1110. https://doi.org/10.1109/infocom52122.2024.10621375
- [53] Jianhao Wang, Zhizhou Ren, Terry Liu, Yang Yu, and Chongjie Zhang. 2020. Qplex: Duplex dueling multi-agent q-learning. arXiv preprint arXiv:2008.01062 (2020).
- Jing Wang, Yu Xuan Wu, Yang-Quan Chen, and Shuang Ju. 2022. Multi-UAVs collaborative tracking of moving target with maximized visibility in urban environment. Journal of the Franklin Institute 359, 11 (2022), 5512-5532.
- [55] Liang Wang, Dingqi Yang, Zhiwen Yu, Fei Xiong, Lei Han, Shirui Pan, and Bin Guo. 2023. Task Scheduling in Three-Dimensional Spatial Crowdsourcing: A Social Welfare Perspective. IEEE Trans. Mob. Comput. 22, 9 (2023), 5555-5567. https://doi.org/10.1109/TMC.2022.
- [56] Yu Wang, Chi Harold Liu, Chengzhe Piao, Ye Yuan, Rui Han, Guoren Wang, and Jian Tang. 2022. Human-drone collaborative spatial crowdsourcing by memory-augmented and distributed multi-agent deep reinforcement learning. In 2022 IEEE 38th International

- Conference on Data Engineering (ICDE). IEEE, 459-471.
- [57] Yu Wang, Jingfei Wu, Xingyuan Hua, Chi Harold Liu, Guozheng Li, Jianxin Zhao, Ye Yuan, and Guoren Wang. 2023. Air-ground spatial crowdsourcing with UAV carriers by geometric graph convolutional multi-agent deep reinforcement learning. In 2023 IEEE 39th International Conference on Data Engineering (ICDE). IEEE, 1790–1802.
- [58] Zhenning Wang, Yue Cao, Kai Jiang, Huan Zhou, Jiawen Kang, Yuan Zhuang, Daxin Tian, and Victor C. M. Leung. 2024. When Crowdsensing Meets Smart Cities: A Comprehensive Survey and New Perspectives. *IEEE Communications Surveys & Tutorials* (2024), 1–1. https://doi.org/10.1109/COMST.2024.3400121
- [59] Yu Wu. 2022. Task scheduling of the collaborative aerial–ground system for the search and capture of multiple targets. Knowledge-Based Systems 250 (2022), 109031.
- [60] Yu Wu, Shaobo Wu, and Xinting Hu. 2020. Cooperative path planning of UAVs & UGVs for a persistent surveillance task in urban environments. *IEEE Internet of Things Journal* 8, 6 (2020), 4906–4919.
- [61] Ying Xu, Xiaobo Li, Xiangpei Meng, and Weipeng Zhang. 2024. An iterated greedy heuristic for collaborative human-uav search of missing tourists. Knowledge-Based Systems 286 (2024), 111409.
- [62] Dingkang Yang, Kun Yang, Yuzheng Wang, Jing Liu, Zhi Xu, Rongbin Yin, Peng Zhai, and Lihua Zhang. 2023. How2comm: Communication-efficient and collaboration-pragmatic multi-agent perception. Advances in Neural Information Processing Systems 36 (2023), 25151–25164.
- [63] Yuxiao Ye, Chi Harold Liu, Zipeng Dai, Jianxin Zhao, Ye Yuan, Guoren Wang, and Jian Tang. 2023. Exploring both individuality and cooperation for air-ground spatial crowdsourcing by multi-agent deep reinforcement learning. In 2023 IEEE 39th International Conference on Data Engineering (ICDE). IEEE, 205–217.
- [64] Zhiyong Yu, Lei Han, Chao Chen, Wenzhong Guo, and Zhiwen Yu. 2021. Object tracking by the least spatiotemporal searches. *IEEE Internet of Things Journal* 8, 16 (2021), 12934–12946.
- [65] Yuan Yuan, Jingtao Ding, Jie Feng, Depeng Jin, and Yong Li. 2024. Unist: A prompt-empowered universal model for urban spatio-temporal prediction. In Proceedings of the 30th ACM SIGKDD Conference on Knowledge Discovery and Data Mining. 4095–4106.
- [66] Zheng Zang, Xi Zhang, Jiarui Song, Yaomin Lu, Zhiwei Li, Haotian Dong, Yuanyuan Li, Zhiyang Ju, and Jianwei Gong. 2024. A coordinated behavior planning and trajectory planning framework for multi-ugvs in unstructured narrow interaction scenarios. IEEE Transactions on Intelligent Vehicles (2024).
- [67] Enze Zhang, Huaze Tang, Xiao-Ping Zhang, and Wenbo Ding. 2025. Mean-Field Aided QMIX: A Scalable and Flexible Q-Learning Approach for Large-Scale Agent Groups. In ICASSP 2025 - 2025 IEEE International Conference on Acoustics, Speech and Signal Processing (ICASSP). 1–5. https://doi.org/10.1109/ICASSP49660.2025.10887881
- [68] Miaomiao Zhang, Wei Tong, Guangyu Zhu, Xin Xu, and Edmond Q Wu. 2024. SQIX: QMIX algorithm activated by general softmax operator for cooperative multiagent reinforcement learning. IEEE Transactions on Systems, Man, and Cybernetics: Systems 54, 11 (2024), 6550–6560
- [69] Yinuo Zhao, Chi Harold Liu, Tianjiao Yi, Guozheng Li, and Dapeng Wu. 2024. Energy-Efficient Ground-Air-Space Vehicular Crowdsensing by Hierarchical Multi-Agent Deep Reinforcement Learning with Diffusion Models. *IEEE Journal on Selected Areas in Communications* (2024).
- [70] Yinuo Zhao, Kun Wu, Zhiyuan Xu, Zhengping Che, Qi Lu, Jian Tang, and Chi Harold Liu. 2022. Cadre: A cascade deep reinforcement learning framework for vision-based autonomous urban driving. In Proceedings of the AAAI conference on artificial intelligence, Vol. 36. 3481–3489
- [71] Yu Zheng, Licia Capra, Ouri Wolfson, and Hai Yang. 2014. Urban computing: concepts, methodologies, and applications. ACM Transactions on Intelligent Systems and Technology (TIST) 5, 3 (2014), 1–55.
- [72] Yu-Jun Zheng, Yi-Chen Du, Hai-Feng Ling, Wei-Guo Sheng, and Sheng-Yong Chen. 2019. Evolutionary collaborative human-UAV search for escaped criminals. *IEEE Transactions on Evolutionary Computation* 24, 2 (2019), 217–231.
- [73] Yu-Jun Zheng, Yi-Chen Du, Zheng-Lian Su, Hai-Feng Ling, Min-Xia Zhang, and Sheng-Yong Chen. 2020. Evolutionary human-UAV cooperation for transmission network restoration. *IEEE Transactions on Industrial Informatics* 17, 3 (2020), 1648–1657.
- [74] Zhenyu Zhou, Junhao Feng, Bo Gu, Bo Ai, Shahid Mumtaz, Jonathan Rodriguez, and Mohsen Guizani. 2018. When mobile crowd sensing meets UAV: Energy-efficient task assignment and route planning. IEEE Transactions on Communications 66, 11 (2018), 5526–5538.
- [75] Xinkai Zuo, Jian Zhou, Fan Yang, Fei Su, Haihong Zhu, and Lin Li. 2023. Real-time global action planning for unmanned ground vehicle exploration in three-dimensional spaces. Expert Systems with Applications 215 (2023), 119264.

A Np-hard Proof

Lemma 1: Problem 1 is NP-Hard.

Proof: To facilitate the NP-Hardness proof, we consider a restricted version of **Problem 1** by making the following assumptions: UAVs have unlimited endurance and are not constrained by vehicles or charging points; UAVs can independently complete tasks without the need for workers; A task task $_x$ is instantly completed

when a UAV arrives at its location $tLoc_x$, with no additional cost:

$$task_x = \emptyset$$
, if $uLoc_i = tLoc_x$

Based on the above, **Problem 1** simplifies to **Problem 2** :

$$\begin{aligned} \textbf{confirm} \ \{A_u_i^{t \times Interval}\}, (t = 0, 1, 2, \dots, \ t \times Interval \in [0, LimitTime]) \\ \textbf{maximize} \ Cplt_Tasks \\ s.t. \ \text{assumptions} \ (3) \end{aligned}$$

Since Problem 2 is a special case of Problem 1 with simpler constraints, Problem 2 can be reduced to **Problem 1. Problem 2** aims to determine the scheduling actions of multiple UAVs to maximize *Cplt_Tasks*, which is a sequential optimal subset selection problem. Since the optimal subset selection problem is known to be NP-Hard [40], **Problem 1** is also NP-Hard.

Detailed experimental setup

We comprehensively evaluate the performance of the proposed algorithm based on real and simulated datasets. The detailed description of the datasets is as follows.

Dataset Settings B.1

- B.1.1 Real Datasets. Real data comes from actual scenarios, which can reflect task distribution, agent behavior patterns, and resource limitations in real environments. The real datasets include bicycle riding order data (BicycleOrder) [24, 71], Didi order data (DidiOrders) [6], and taxi trajectory data (TaxiTrajectories) [64]. First, we discretize the coverage area of the real datasets. Then, we filter, classify, and annotate the data to obtain data that meets the experimental specifications. The specific processing procedures can be referred to in [5].
- B.1.2 Random Simulated Datasets. Random simulated datasets are generated through parameterization, which can flexibly adjust area scale, task quantity, agent scale, etc., to verify the algorithm's performance in different scenarios. The introduction of random data compensates for the lack of diversity and controllability in real data. The detailed data generation process can be referred to in [5].

Specifically, the distribution of task points and charging points in the four types of datasets is shown in Fig. 13, with significant differences in their distribution patterns. In addition, the detailed dataset description is shown in Table 5.

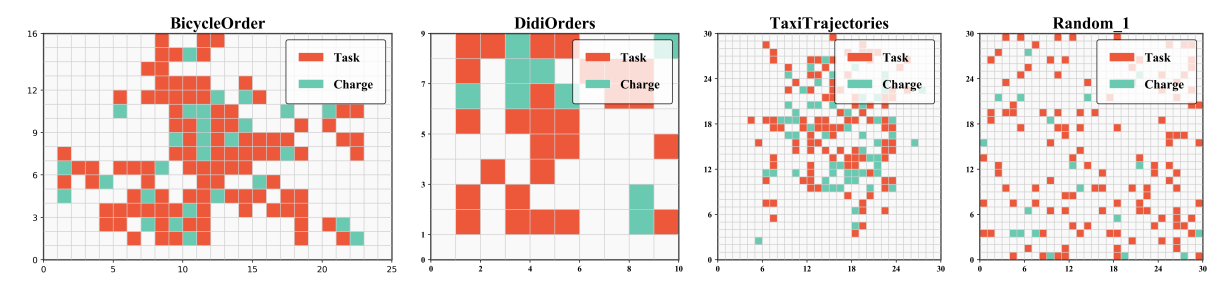


Fig. 13. Distribution of task points and charging points in four types of datasets (the size of each grid is 1KM*1KM).

B.2 Experiment Setup

Based on the above datasets, we set up 5 groups of experiments to comprehensively evaluate the HoCs-MPQ algorithm., as shown in Table 6.

Table 5. Description of experimental datasets

Dataset Area scale number Tasks ord number number number Agent time time Agent time power power power Charging power power BicycleOrder 25 × 16 99 30 >70 min (54,17,34) 3 10 DidiOrders 10 × 9 34 10 >50 min (26,18,14) 3 10 Random_1 30 × 30 102 60 >90 min (38,20,16) 3 10 Random_2 20 × 20 120 20 60 min (50,30,20) 3 10 Random_3 40 × 40 120 20 60 min (50,30,20) 3 10 Random_4 30 × 30 100 20 60 min (50,30,20) 3 10 Random_4 30 × 30 120 10 60 min (50,30,20) 3 10 Random_5 30 × 30 120 10 60 min (50,30,20) 3 10 Random_6 30 × 30 120 20 40 min (50,30,20) 3					<u>'</u>			
BicycleOrder 25 × 16 99 30 >70 min (54,17,34) 3 10 DidiOrders 10 × 9 34 10 >50 min (26,18,14) 3 10 TaxiTrajectories 30 × 30 102 60 >90 min (38,20,16) 3 10 Random_1 30 × 30 120 20 60 min (50,30,20) 3 10 Random_2 20 × 20 120 20 60 min (50,30,20) 3 10 Random_3 40 × 40 120 20 60 min (50,30,20) 3 10 Random_4 30 × 30 100 20 60 min (50,30,20) 3 10 Random_5 30 × 30 120 10 60 min (50,30,20) 3 10 Random_6 30 × 30 120 30 60 min (50,30,20) 3 10 Random_9 30 × 30 120 20 40 min (50,30,20) 3 10	Dataset		Tasks	Charging point	Agents online	Agent	Task cost	Charging
DidiOrders 10 × 9 34 10 >50 min (26,18,14) 3 10 TaxiTrajectories 30 × 30 102 60 >90 min (38,20,16) 3 10 Random_1 30 × 30 120 20 60 min (50,30,20) 3 10 Random_2 20 × 20 120 20 60 min (50,30,20) 3 10 Random_3 40 × 40 120 20 60 min (50,30,20) 3 10 Random_4 30 × 30 100 20 60 min (50,30,20) 3 10 Random_5 30 × 30 140 20 60 min (50,30,20) 3 10 Random_6 30 × 30 120 30 60 min (50,30,20) 3 10 Random_7 30 × 30 120 20 40 min (50,30,20) 3 10 Random_9 30 × 30 120 20 80 min (50,30,20) 3 10		scale					power	power
TaxiTrajectories 30 × 30 102 60 >90 min (38,20,16) 3 10 Random_1 30 × 30 120 20 60 min (50,30,20) 3 10 Random_2 20 × 20 120 20 60 min (50,30,20) 3 10 Random_3 40 × 40 120 20 60 min (50,30,20) 3 10 Random_4 30 × 30 100 20 60 min (50,30,20) 3 10 Random_5 30 × 30 140 20 60 min (50,30,20) 3 10 Random_6 30 × 30 120 10 60 min (50,30,20) 3 10 Random_7 30 × 30 120 20 40 min (50,30,20) 3 10 Random_9 30 × 30 120 20 80 min (50,30,20) 3 10 Random_10 30 × 30 120 20 60 min (50,30,20) 3 10				30	>70 min	(54,17,34)	3	10
Random_1 30 × 30 120 20 60 min (50,30,20) 3 10 Random_2 20 × 20 120 20 60 min (50,30,20) 3 10 Random_3 40 × 40 120 20 60 min (50,30,20) 3 10 Random_4 30 × 30 100 20 60 min (50,30,20) 3 10 Random_5 30 × 30 140 20 60 min (50,30,20) 3 10 Random_6 30 × 30 120 10 60 min (50,30,20) 3 10 Random_6 30 × 30 120 30 60 min (50,30,20) 3 10 Random_7 30 × 30 120 20 40 min (50,30,20) 3 10 Random_8 30 × 30 120 20 80 min (50,30,20) 3 10 Random_10 30 × 30 120 20 60 min (50,30,20) 3 10 Ra	DidiOrders	10×9	34	10	>50 min	(26,18,14)	3	10
Random_2 20 × 20 120 20 60 min (50,30,20) 3 10 Random_3 40 × 40 120 20 60 min (50,30,20) 3 10 Random_4 30 × 30 100 20 60 min (50,30,20) 3 10 Random_5 30 × 30 140 20 60 min (50,30,20) 3 10 Random_6 30 × 30 120 10 60 min (50,30,20) 3 10 Random_7 30 × 30 120 30 60 min (50,30,20) 3 10 Random_8 30 × 30 120 20 40 min (50,30,20) 3 10 Random_9 30 × 30 120 20 40 min (50,30,20) 3 10 Random_10 30 × 30 120 20 60 min (50,30,20) 3 10 Random_11 30 × 30 120 20 60 min (50,30,20) 3 10 R	TaxiTrajectories	30×30	102	60	>90 min	(38,20,16)	3	10
Random_3 40 × 40 120 20 60 min (50,30,20) 3 10 Random_4 30 × 30 100 20 60 min (50,30,20) 3 10 Random_5 30 × 30 140 20 60 min (50,30,20) 3 10 Random_6 30 × 30 120 10 60 min (50,30,20) 3 10 Random_6 30 × 30 120 30 60 min (50,30,20) 3 10 Random_7 30 × 30 120 20 40 min (50,30,20) 3 10 Random_8 30 × 30 120 20 80 min (50,30,20) 3 10 Random_9 30 × 30 120 20 80 min (50,30,20) 3 10 Random_10 30 × 30 120 20 60 min (70,40,30) 3 10 Random_11 30 × 30 120 20 60 min (70,30,20) 3 10 R	Random_1	30×30	120	20	60 min	(50,30,20)	3	10
Random_4 30 × 30 100 20 60 min (50,30,20) 3 10 Random_5 30 × 30 140 20 60 min (50,30,20) 3 10 Random_6 30 × 30 120 10 60 min (50,30,20) 3 10 Random_7 30 × 30 120 30 60 min (50,30,20) 3 10 Random_8 30 × 30 120 20 40 min (50,30,20) 3 10 Random_9 30 × 30 120 20 80 min (50,30,20) 3 10 Random_10 30 × 30 120 20 60 min (30,20,10) 3 10 Random_11 30 × 30 120 20 60 min (70,40,30) 3 10 Random_12 30 × 30 120 20 60 min (70,30,20) 3 10 Random_13 30 × 30 120 20 60 min (50,40,20) 3 10 <td< td=""><td>Random_2</td><td>20×20</td><td>120</td><td>20</td><td>60 min</td><td>(50,30,20)</td><td>3</td><td>10</td></td<>	Random_2	20×20	120	20	60 min	(50,30,20)	3	10
Random_5 30 × 30 140 20 60 min (50,30,20) 3 10 Random_6 30 × 30 120 10 60 min (50,30,20) 3 10 Random_7 30 × 30 120 30 60 min (50,30,20) 3 10 Random_8 30 × 30 120 20 40 min (50,30,20) 3 10 Random_9 30 × 30 120 20 80 min (50,30,20) 3 10 Random_10 30 × 30 120 20 60 min (30,20,10) 3 10 Random_11 30 × 30 120 20 60 min (70,40,30) 3 10 Random_11 30 × 30 120 20 60 min (70,40,30) 3 10 Random_12 30 × 30 120 20 60 min (70,30,20) 3 10 Random_13 30 × 30 120 20 60 min (50,40,20) 3 10 <t< td=""><td>Random_3</td><td>40×40</td><td>120</td><td>20</td><td>60 min</td><td>(50,30,20)</td><td>3</td><td>10</td></t<>	Random_3	40×40	120	20	60 min	(50,30,20)	3	10
Random_6 30 × 30 120 10 60 min (50,30,20) 3 10 Random_7 30 × 30 120 30 60 min (50,30,20) 3 10 Random_8 30 × 30 120 20 40 min (50,30,20) 3 10 Random_9 30 × 30 120 20 80 min (50,30,20) 3 10 Random_10 30 × 30 80 20 60 min (30,20,10) 3 10 Random_11 30 × 30 120 20 60 min (70,40,30) 3 10 Random_12 30 × 30 120 20 60 min (30,30,20) 3 10 Random_13 30 × 30 120 20 60 min (50,20,20) 3 10 Random_14 30 × 30 120 20 60 min (50,40,20) 3 10 Random_15 30 × 30 120 20 60 min (50,30,30) 3 10 <t< td=""><td>Random_4</td><td>30×30</td><td>100</td><td>20</td><td>60 min</td><td>(50,30,20)</td><td>3</td><td>10</td></t<>	Random_4	30×30	100	20	60 min	(50,30,20)	3	10
Random_7 30 × 30 120 30 60 min (50,30,20) 3 10 Random_8 30 × 30 120 20 40 min (50,30,20) 3 10 Random_9 30 × 30 120 20 80 min (50,30,20) 3 10 Random_10 30 × 30 80 20 60 min (30,20,10) 3 10 Random_11 30 × 30 120 20 60 min (70,40,30) 3 10 Random_12 30 × 30 120 20 60 min (30,30,20) 3 10 Random_13 30 × 30 120 20 60 min (70,30,20) 3 10 Random_14 30 × 30 120 20 60 min (50,40,20) 3 10 Random_15 30 × 30 120 20 60 min (50,40,20) 3 10 Random_16 30 × 30 120 20 60 min (50,30,30) 3 10 <	Random_5	30×30	140	20	60 min	(50,30,20)	3	10
Random_8 30 × 30 120 20 40 min (50,30,20) 3 10 Random_9 30 × 30 120 20 80 min (50,30,20) 3 10 Random_10 30 × 30 80 20 60 min (30,20,10) 3 10 Random_11 30 × 30 120 20 60 min (70,40,30) 3 10 Random_12 30 × 30 120 20 60 min (30,30,20) 3 10 Random_13 30 × 30 120 20 60 min (70,30,20) 3 10 Random_14 30 × 30 120 20 60 min (50,20,20) 3 10 Random_15 30 × 30 120 20 60 min (50,40,20) 3 10 Random_16 30 × 30 120 20 60 min (50,30,10) 3 10 Random_17 30 × 30 120 20 60 min (50,30,20) 2 10	Random_6	30×30	120	10	60 min	(50,30,20)	3	10
Random_9 30 × 30 120 20 80 min (50,30,20) 3 10 Random_10 30 × 30 80 20 60 min (30,20,10) 3 10 Random_11 30 × 30 120 20 60 min (70,40,30) 3 10 Random_12 30 × 30 120 20 60 min (30,30,20) 3 10 Random_13 30 × 30 120 20 60 min (70,30,20) 3 10 Random_14 30 × 30 120 20 60 min (50,20,20) 3 10 Random_15 30 × 30 120 20 60 min (50,40,20) 3 10 Random_16 30 × 30 120 20 60 min (50,30,10) 3 10 Random_17 30 × 30 120 20 60 min (50,30,10) 3 10 Random_18 30 × 30 120 20 60 min (50,30,30) 3 10 Random_19 30 × 30 120 20 60 min (50,30,20) 2 10 Random_19 30 × 30 120 20 60 min (50,30,20) 2 10 Random_19 30 × 30 120 20 60 min (50,30,20) 4 10 Random_20 30 × 30 120 20 60 min (50,30,20) [2,3] 10 Random_21 30 × 30 120 20 60 min (50,30,20) [2,3] 10 Random_22 30 × 30 120 20 60 min (50,30,20) [3,4] 10 Random_22 30 × 30 120 20 60 min (50,30,20) [4,5] 10 Random_22 30 × 30 120 20 60 min (50,30,20) [4,5] 10 Random_23 30 × 30 120 20 60 min (50,30,20) 3 6 Random_24 30 × 30 120 20 60 min (50,30,20) 3 6 Random_25 30 × 30 120 20 60 min (50,30,20) 3 [2,6] Random_26 30 × 30 120 20 60 min (50,30,20) 3 [2,6] Random_27 30 × 30 120 20 60 min (50,30,20) 3 [2,6] Random_27 30 × 30 120 20 60 min (50,30,20) 3 [2,6] Random_27 30 × 30 120 20 60 min (50,30,20) 3 [2,6] Random_27 30 × 30 120 20 60 min (50,30,20) 3 [2,6] Random_27 30 × 30 120 20 60 min (50,30,20) 3 [2,6] Random_27 30 × 30 120 20 60 min (50,30,20) 3 [6,10] Random_27 30 × 30 120 20 60 min (50,30,20) 3 [10,14] Random_28 40 × 40 240 40 60 min (50,30,20) 3 [10,14]	Random_7	30×30	120	30	60 min	(50,30,20)	3	10
Random_10 30 × 30 80 20 60 min (30,20,10) 3 10 Random_11 30 × 30 120 20 60 min (70,40,30) 3 10 Random_12 30 × 30 120 20 60 min (30,30,20) 3 10 Random_13 30 × 30 120 20 60 min (70,30,20) 3 10 Random_14 30 × 30 120 20 60 min (50,20,20) 3 10 Random_15 30 × 30 120 20 60 min (50,40,20) 3 10 Random_16 30 × 30 120 20 60 min (50,30,10) 3 10 Random_17 30 × 30 120 20 60 min (50,30,30) 3 10 Random_18 30 × 30 120 20 60 min (50,30,20) 2 10 Random_20 30 × 30 120 20 60 min (50,30,20) [2,3] 10	Random_8	30×30	120	20	40 min	(50,30,20)	3	10
Random_11 30 × 30 120 20 60 min (70,40,30) 3 10 Random_12 30 × 30 120 20 60 min (30,30,20) 3 10 Random_13 30 × 30 120 20 60 min (70,30,20) 3 10 Random_14 30 × 30 120 20 60 min (50,20,20) 3 10 Random_15 30 × 30 120 20 60 min (50,40,20) 3 10 Random_16 30 × 30 120 20 60 min (50,30,10) 3 10 Random_17 30 × 30 120 20 60 min (50,30,30) 3 10 Random_18 30 × 30 120 20 60 min (50,30,20) 2 10 Random_29 30 × 30 120 20 60 min (50,30,20) [2,3] 10 Random_21 30 × 30 120 20 60 min (50,30,20) [3,4] 10 <t< td=""><td>Random_9</td><td>30×30</td><td>120</td><td>20</td><td>80 min</td><td>(50,30,20)</td><td>3</td><td>10</td></t<>	Random_9	30×30	120	20	80 min	(50,30,20)	3	10
Random_12 30 × 30 120 20 60 min (30,30,20) 3 10 Random_13 30 × 30 120 20 60 min (70,30,20) 3 10 Random_14 30 × 30 120 20 60 min (50,20,20) 3 10 Random_15 30 × 30 120 20 60 min (50,40,20) 3 10 Random_16 30 × 30 120 20 60 min (50,30,10) 3 10 Random_17 30 × 30 120 20 60 min (50,30,30) 3 10 Random_18 30 × 30 120 20 60 min (50,30,20) 2 10 Random_19 30 × 30 120 20 60 min (50,30,20) 2 10 Random_20 30 × 30 120 20 60 min (50,30,20) [2,3] 10 Random_21 30 × 30 120 20 60 min (50,30,20) [4,5] 10 <t< td=""><td>Random_10</td><td>30×30</td><td>80</td><td>20</td><td>60 min</td><td>(30,20,10)</td><td>3</td><td>10</td></t<>	Random_10	30×30	80	20	60 min	(30,20,10)	3	10
Random_13 30 × 30 120 20 60 min (70,30,20) 3 10 Random_14 30 × 30 120 20 60 min (50,20,20) 3 10 Random_15 30 × 30 120 20 60 min (50,40,20) 3 10 Random_16 30 × 30 120 20 60 min (50,30,10) 3 10 Random_17 30 × 30 120 20 60 min (50,30,30) 3 10 Random_18 30 × 30 120 20 60 min (50,30,20) 2 10 Random_19 30 × 30 120 20 60 min (50,30,20) 2 10 Random_20 30 × 30 120 20 60 min (50,30,20) [2,3] 10 Random_21 30 × 30 120 20 60 min (50,30,20) [3,4] 10 Random_22 30 × 30 120 20 60 min (50,30,20) [4,5] 10	Random_11	30×30	120	20	60 min	(70,40,30)	3	10
Random_14	Random_12	30×30	120	20	60 min	(30,30,20)	3	10
Random_15	Random_13	30×30	120	20	60 min	(70,30,20)	3	10
Random_16	Random_14	30×30	120	20	60 min	(50,20,20)	3	10
Random_17 30 × 30 120 20 60 min (50,30,30) 3 10 Random_18 30 × 30 120 20 60 min (50,30,20) 2 10 Random_19 30 × 30 120 20 60 min (50,30,20) 4 10 Random_20 30 × 30 120 20 60 min (50,30,20) [2,3] 10 Random_21 30 × 30 120 20 60 min (50,30,20) [3,4] 10 Random_22 30 × 30 120 20 60 min (50,30,20) [3,4] 10 Random_22 30 × 30 120 20 60 min (50,30,20) [4,5] 10 Random_23 30 × 30 120 20 60 min (50,30,20) 3 6 Random_24 30 × 30 120 20 60 min (50,30,20) 3 14 Random_25 30 × 30 120 20 60 min (50,30,20) 3 14 Random_26 30 × 30 120 20 60 min (50,30,20) 3 [2,6] Random_26 30 × 30 120 20 60 min (50,30,20) 3 [6,10] Random_27 30 × 30 120 20 60 min (50,30,20) 3 [10,14] Random_28 40 × 40 240 40 60 min (100,60,40) 3 10	Random_15	30×30	120	20	60 min	(50,40,20)	3	10
Random_18 30 × 30 120 20 60 min (50,30,20) 2 10 Random_19 30 × 30 120 20 60 min (50,30,20) 4 10 Random_20 30 × 30 120 20 60 min (50,30,20) [2,3] 10 Random_21 30 × 30 120 20 60 min (50,30,20) [3,4] 10 Random_22 30 × 30 120 20 60 min (50,30,20) [4,5] 10 Random_23 30 × 30 120 20 60 min (50,30,20) 3 6 Random_24 30 × 30 120 20 60 min (50,30,20) 3 14 Random_25 30 × 30 120 20 60 min (50,30,20) 3 [6,10] Random_26 30 × 30 120 20 60 min (50,30,20) 3 [6,10] Random_27 30 × 30 120 20 60 min (50,30,20) 3 [10,14]	Random_16	30×30	120	20	60 min	(50,30,10)	3	10
$\begin{array}{cccccccccccccccccccccccccccccccccccc$	Random_17	30×30	120	20	60 min	(50,30,30)	3	10
$\begin{array}{cccccccccccccccccccccccccccccccccccc$	Random_18	30×30	120	20	60 min	(50,30,20)	2	10
Random_21 30 × 30 120 20 60 min (50,30,20) [3,4] 10 Random_22 30 × 30 120 20 60 min (50,30,20) [4,5] 10 Random_23 30 × 30 120 20 60 min (50,30,20) 3 6 Random_24 30 × 30 120 20 60 min (50,30,20) 3 14 Random_25 30 × 30 120 20 60 min (50,30,20) 3 [2,6] Random_26 30 × 30 120 20 60 min (50,30,20) 3 [6,10] Random_27 30 × 30 120 20 60 min (50,30,20) 3 [10,14] Random_28 40 × 40 240 40 60 min (100,60,40) 3 10	Random_19	30×30	120	20	60 min	(50,30,20)	4	10
Random_22 30 × 30 120 20 60 min (50,30,20) [4,5] 10 Random_23 30 × 30 120 20 60 min (50,30,20) 3 6 Random_24 30 × 30 120 20 60 min (50,30,20) 3 14 Random_25 30 × 30 120 20 60 min (50,30,20) 3 [2,6] Random_26 30 × 30 120 20 60 min (50,30,20) 3 [6,10] Random_27 30 × 30 120 20 60 min (50,30,20) 3 [10,14] Random_28 40 × 40 240 40 60 min (100,60,40) 3 10	Random_20	30×30	120	20	60 min	(50,30,20)	[2,3]	10
Random_23 30 × 30 120 20 60 min (50,30,20) 3 6 Random_24 30 × 30 120 20 60 min (50,30,20) 3 14 Random_25 30 × 30 120 20 60 min (50,30,20) 3 [2,6] Random_26 30 × 30 120 20 60 min (50,30,20) 3 [6,10] Random_27 30 × 30 120 20 60 min (50,30,20) 3 [10,14] Random_28 40 × 40 240 40 60 min (100,60,40) 3 10	Random_21	30×30	120	20	60 min	(50,30,20)	[3,4]	10
$\begin{array}{cccccccccccccccccccccccccccccccccccc$	Random_22	30×30	120	20	60 min	(50,30,20)	[4,5]	10
$\begin{array}{cccccccccccccccccccccccccccccccccccc$	Random_23	30×30	120	20	60 min	(50,30,20)	3	6
$\begin{array}{c ccccccccccccccccccccccccccccccccccc$	Random_24	30×30	120	20	60 min	(50,30,20)	3	14
Random_27 30 × 30 120 20 60 min (50,30,20) 3 [10,14] Random_28 40 × 40 240 40 60 min (100,60,40) 3 10	Random_25	30×30	120	20	60 min	(50,30,20)	3	[2,6]
Random_28 40 × 40 240 40 60 min (100,60,40) 3 10	Random_26	30×30	120	20	60 min	(50,30,20)	3	[6,10]
	Random_27	30×30	120	20	60 min	(50,30,20)	3	[10,14]
Random_29 60 × 60 480 80 60 min (200,120,80) 3 10	Random_28	40×40	240	40	60 min	(100,60,40)	3	10
	Random_29	60×60	480	80	60 min	(200,120,80)	3	10

B.3 Comparison Methods

B.3.1 HoCs-GREEDY (Heterogeneous Multi-Agent Online Collaborative Scheduling Algorithm Based on GREEDY). The greedy algorithm adopts a locally optimal strategy for real-time decision-making [22, 55]. It optimizes the movement paths of UAVs, workers, and vehicles in stages. Its core process is divided into three steps: First, plan the path for UAVs, calculate the sum of Euclidean distances from all positions within the selectable moving range to various task points, and select the position with the minimum total distance as the target point for the next moment. Second, perform the same logic for workers, selecting the next position with the shortest total distance to task points. Finally, plan the path for vehicles, calculate the total distance from each position to all UAVs' next target points, and select the minimum value as the vehicle's moving target. All three types of agents complete

Group	Dataset	Interval	Limit time	Controlled variable
(1)	BicycleOrder / DidiOrders / TaxiTrajectories / Random_1	5 min/ 10 min/ 15 min	3 h	Interval
(2)	BicycleOrder / DidiOrders / TaxiTrajectories / Random_1	5 min	2 h/ 3 h/ 4 h	Limit time
(3)	Random_1, Random_2–Random_9	10 min	3 h	Area scale Tasks number Charging point number Agents online time
(4)	Random_1, Random_10-Random_17	10 min	3 h	Workers number UAVs number Vehicles number
(5)	Random_1, Random_18–Random_27	10 min	3 h	Task cost power Charging power

Table 6. Experimental groups and controlled variables

the entire path planning through iterative calculation. This method achieves global path optimization through a cascade of locally optimal choices, suitable for collaborative scenarios of multiple agent types.

B.3.2 HoCs-KWTA (Heterogeneous Multi-Agent Online Collaborative Scheduling Algorithm Based on K-Winners-Take-All). HoCs-KWTA extends from the selective activation mechanism of neural networks and can be used for multi-agent task matching [30, 31, 43]. UAV matching is dimensionally divided into task UAVs and charging UAVs. Taking task matching as an example, task UAVs score task points within their power range, and workers score all task points. The top K high-scoring tasks are retained, and the intersection is checked to determine the ternary matching for collaborative execution. If there is no intersection, suboptimal tasks are tried in descending order of scores. Charging point matching is similar.

B.3.3 HoCs-MADL (Heterogeneous Multi-Agent Online Collaborative Scheduling Algorithm Based on Multi-Agent Deep Learning). Based on a multi-agent deep learning framework [27, 28], HoCs-MADL models the state and action spaces of heterogeneous agents through shared neural networks. Global information (task point distribution, charging point distribution, etc.) is extracted by convolutional networks and then combined with local states (agent position, UAV power, etc.) as input to a deep network. This produces the immediate action value for each agent and uses end-to-end training to optimize the immediate task completion rate. Note that the detailed implementation processes of HoCs-MADL and HoCs-MARL heavily reference [14].

To facilitate this, we introduce the Heterogeneous Multi-Agent Network Framework (MANF), inspired by the factorization principles of the QMIX algorithm. MANF is specifically designed to handle diverse agent types—UAVs, workers, and cars—within a unified computational structure.

As illustrated in Figure 14, MANF primarily consists of two interconnected neural networks: the agent network and the mixing network. The agent network processes observations from individual agents (UAVs, workers, or cars) and outputs their respective individual Q-values, denoted as $Q^t_{ijk}(a^t_{ijk})$. The mixing network then takes these individual $Q^t_{ijk}(a^t_{ijk})$ values as inputs and aggregates them to produce a joint Q-value, $Q^t_{tot}(\mathbf{a}^t)$, representing the value of the joint action for the entire multi-agent system. The parameters (weights and biases) of the mixing

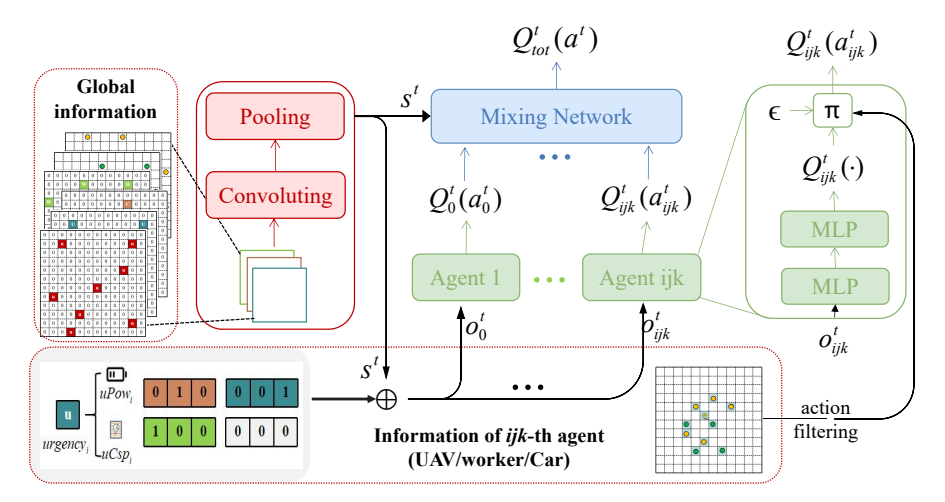


Fig. 14. Heterogeneous multi-agent network framework (MANF).

network are dynamically generated by a hypernetworks architecture. A crucial constraint for the mixing network's weights, derived from its design principles, is that they must always be greater than zero. Fundamentally, MANF processes information through a dual stream: global information, providing a broad environmental context, and local agent information, capturing specific details of each individual agent. This comprehensive information structure feeds into the subsequent route planning algorithms.

Delving deeper into this information structure, the state space within the MANF framework is meticulously defined by categorizing observed information into two distinct types: global environmental information and local agent-specific information.

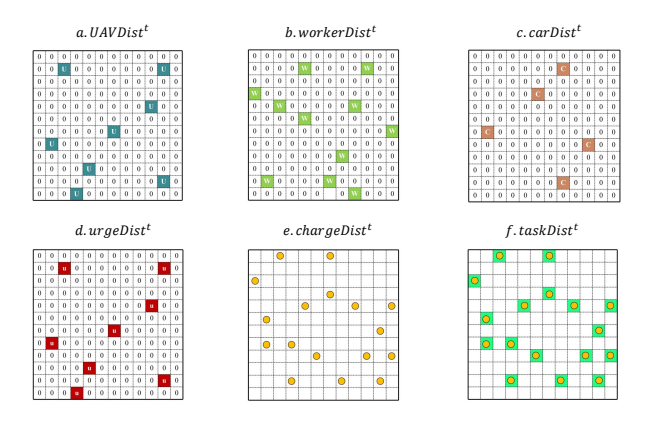


Fig. 15. Global information at the moment t

As conceptually depicted in Figure 15, global information provides a system-wide view of the environment at time t. This includes:

• *UAVDist*^t: Shows the distribution of UAVs at the moment t.

- workDist^t: Shows the distribution of workers at the moment t.
- *carDist*^t: Shows the distribution of cars at the moment t.
- *urgeDist^t*: Shows the urgency distribution to replace UAVs' battery at the moment t, which measures the cumulative urgency of replacing batteries for all UAVs in different locations.
- *taskDist*^t: Shows the distribution of tasks at the moment t.
- *chargeDist*^t: Shows the distribution of chargepoints at the moment t.

These global features are processed by a spatial convolutional neural network (CNN), specifically 'cnnSpace', to extract meaningful spatial embeddings, which are then shared among all heterogeneous agents as part of the global state s^t .

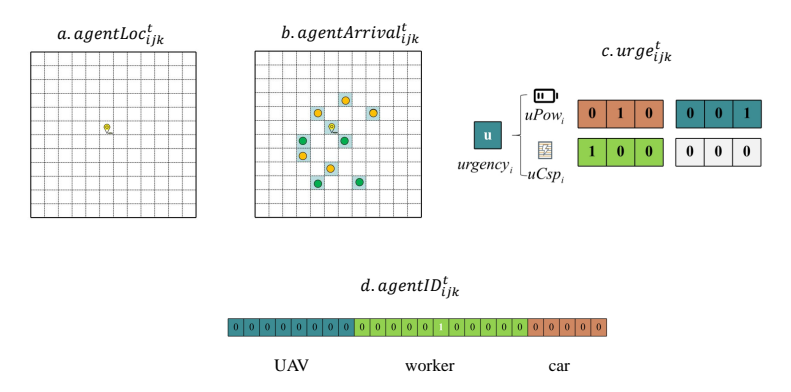


Fig. 16. Local information of the ijk agent at the moment t

As illustrated in Figure 16, local information provides specific details pertinent to individual agents (UAVs, workers, and cars) at time *t*. This comprises:

- $agentLoc_{ijk}^t$: The precise geographical location of the ijk-th agent.
- $agentArrival_{ijk}^t$: Represents the set of reachable areas for the ijk-th agent within the forthcoming time step [t, t+1). These movement ranges are predefined and already exclude physically unreachable locations.
- urge^t_{ijk}: The urgency of the ijk-th agent to replace its battery at time t. Workers and cars are assumed
 to have infinite power, so their urgency is zero. For UAVs, urge^t_{ijk} is determined such that higher current
 power leads to lower urgency, and the rate of urgency decrease diminishes as power increases.
- agentID^t_{ijk}: The unique identification number of the ijk-th agent, typically implemented using one-hot encoding.

This local information, along with the global state s^t derived from the CNN, is concatenated to form the comprehensive input o_{ijk}^t for each agent's evaluation network ('evalAgent').

With the state space clearly defined, the HoCs-MADL algorithm, effectively leveraging the MANF architecture, executes its core logic. This heterogeneous multi-agent route planning approach, built upon deep learning principles, is designed to identify the optimal action within a specific time step. The process begins by calculating the expected immediate reward for selecting a set of actions, such as $\{a_t^0,...,a_{ijk}^t,...\}$, given the current state, characterized by observations like $\{o_t^0,...,o_{ijk}^t,...\}$, all within the time interval [t,t+1). This immediate reward is comprehensively composed of two essential elements: the successful completion of sensing tasks and the reduction in urgency. Following this calculation, the algorithm precisely establishes a ternary mapping relationship that effectively links the current state, the chosen actions, and their corresponding immediate reward. This established

mapping then serves as the foundation for training the deep neural network. Through this training phase, the network learns to accurately predict the expected immediate reward when presented with a current state and potential actions. Finally, leveraging the capabilities of the trained model, the system can compare the anticipated immediate rewards for various actions under the existing state, ultimately selecting the action that yields the highest expected reward. This selection process is iterated until the designated target moment is achieved. It is important to note that the target values for rewards in this approach are directly derived from objective real-world environments, ensuring their stability and freedom from bias.

B.3.4 HoCs-MARL (Heterogeneous Multi-Agent Online Collaborative Scheduling Algorithm Based on Multi-Agent Reinforcement Learning). Multi-agent reinforcement learning optimizes long-term cumulative rewards through collaborative strategies [56, 63, 70]. Referencing the QMIX algorithm, it designs a mixing network that fuses the local Q values of each agent, constraining weights to be non-negative to maintain monotonicity. Agents balance "exploration-exploitation" between immediate returns and future collaboration potential. The reward function focuses on the number of completed tasks, avoiding short-term interference from charging gains. Target networks are introduced to mitigate training instability issues, supporting complex spatiotemporal collaborative decision-making.

The HoCs-MARL algorithm extends the capabilities by incorporating the long-term implications of current observations on subsequent action choices. This algorithm estimates the total expected immediate reward over an extended time horizon. While the basic immediate reward can be derived, a critical adjustment is made to align it more closely with the overall optimization objective, which typically aims to maximize total task completion. This refinement is crucial because the impact of certain factors, such as car contributions to battery replacement, may have a delayed effect, influencing future task completion rates. To address potential training instability often seen with single neural networks, such as biased estimations and escalating discrepancies during updates, HoCs-MARL integrates a target network and an evaluation network. The evaluation network is continuously updated based on ongoing learning, while the target network, which provides more stable target values, is periodically synchronized with the evaluation network. This slower update mechanism for the target network helps to stabilize the learning process by ensuring that the target values change gradually, thereby facilitating more consistent and robust learning for the agents. Through these mechanisms, HoCs-MARL enables agents to make decisions that consider both immediate benefits and long-term strategic outcomes in complex routing scenarios.

Otherwise, HoCs MADL/MARL are implemented on the QMIX architecture and thus are only suitable for scenarios where the number and types of agents are fixed. This is because the structure and weights of QMIX's mixing network directly depend on fixed parameters. When the number of agents changes (i.e., the coupling relationships among agents change), the mixing network cannot automatically adapt, causing the model to fail to varying degrees. Introducing attention mechanisms and hierarchical architectures can partially address the problem of dynamic agent composition. For example, Ai-qmix[17] employs a self-attention module to dynamically compute cooperation weights among agents, allowing the mixing network to adjust its focus on different agents' Q-values according to the current scenario. The COPA[26] framework uses a hierarchical architecture—where the coach encodes the global state using global observations combined with multi-head attention and generates strategy vectors tailored for each player, and each player processes its own local observations with multi-head attention—to adapt to a variable number of agents, supporting coordination and zero-shot generalization when agents dynamically join or leave.

However, we did not further customize HoCs MADL/MARL based on related literature for two reasons. (1) Disasters are extreme and rare events that require immediate response, whereas reinforcement learning-based solutions require time to model the environment and train the model, making them unsuitable for disaster scenarios. (2) In practice, we do not yet know how to integrate attention mechanisms and hierarchical architectures

into HoCs MADL/MARL in a way that fits our problem. Furthermore, developing a more deeply customized version of HoCs MADL/MARL for the specific problem addressed in this paper is beyond the scope of our research. We have instead identified and used the latest methods for comparison.

B.3.5 LLM (Large Language Model). Given the excellent generalization properties and immediate reasoning capabilities demonstrated by large language models in handling combinatorial optimization problems, we exploratively designed an online scheduling mechanism based on LLMs [25, 65]. The problem description is converted into natural language input, and the large model generates scheduling plans in real-time. For our problem, the detailed natural language prompts sent to the large model can be referred to in [5].

However, after in-depth interaction with multiple mainstream large language models and repeated experiments, we observed obvious limitations in current models when handling multi-constraint scheduling tasks in complex post-disaster environments. Although the models perform well at the language understanding level, they still fall short in integrating task backgrounds, abstracting multi-source constraint conditions, and generating reasonable scheduling plans accordingly. The scheduling behaviors generated by the models often lack logical consistency, and deviations or even obvious errors easily occur in the reasoning chain, making it difficult to meet the actual requirements of such high-complexity tasks.

Comparison with Contemporary Deep and Reinforcement Learning Methods

C.1 Method Description

C.1.1 QMIX. The QMIX algorithm represents a significant advancement in multi-agent reinforcement learning (MARL), specifically designed to facilitate cooperation among multiple agents by factorizing the joint actionvalue function. A key characteristic of QMIX is its emphasis on monotonic factorization, which implies that the global Q-value monotonically increases with respect to each agent's individual Q-value. This property is crucial as it allows for decentralized policy execution while ensuring consistency with a centralized learner, thereby promoting efficient and stable learning in cooperative multi-agent environments. In the comprehensive comparative experiments conducted against other QMIX-based algorithms, the HoCs-MARL algorithm is utilized for performance evaluation.

C.1.2 QPLEX. This method augments QMIX's mixing network with a dual-stream architecture, comprising an advantage stream for individual advantage function computation and a state stream for global state encoding. These streams' outputs are connected via a learnable weight matrix.

QPLEX decomposes the joint Q-value into a state value and weighted advantage terms:

$$Q_{tot}(s, \mathbf{a}) = V_{mix}(s) + \sum_{i=1}^{n} w_i(s, \mathbf{a}) \cdot A_i(o_i, a_i)$$

where:

- $\bullet \ A_i(o_i, a_i) = Q_i(o_i, a_i) V_i(o_i)$
- $w_i(s, \mathbf{a}) \ge 0$ represents the output of a weight network, dependent on state and action, satisfying normalization or non-negative constraints.

C.1.3 QTRAN. This approach removes QMIX's monotonicity constraint and introduces a transformation network to map the joint Q-value into the individual Q-value space. Its implementation necessitates three distinct loss functions: 1) Mean Squared Error (MSE) loss between individual Q-values and the transformation network's output; 2) an optimal action selection constraint; and 3) a feasibility condition constraint.

QTRAN introduces an undecomposed joint Q-function $Q_{tot}^{joint}(s, \mathbf{a})$ and enforces consistency constraints to anchor the decomposed functions to it.

Table 7. Comparison and Characteristics of Common Combinatorial Optimization Algorithms

Category	Algorithm	Brief Description	Advantages	Disadvantages
Heuristic	Greedy Algorithm	Selects the local optimum	Fast and simple to	Prone to local optima;
Methods	(Greedy)	at each step to construct	implement.	unstable solution
		the overall solution.		quality.
	k-Winner-Take-	Selects the top k	Efficient and easy to	Static selection; does not
	All (kWTA)	candidates based on	parallelize.	consider global
		response scores.		optimization.
	Maximum	Builds the optimal task	Leverages graph	Depends on graph
	Weighted	subset by combining	structure; robust and	construction; limited
	Independent Set	node weights and graph	suitable for complex	scalability in large
	Heuristic Search	feasibility constraints.	constraints.	graphs.
	(Ours)			21
Meta-	Genetic	Simulates evolution	Escapes local optima;	Slow convergence; many
Heuristic	Algorithm (GA)	through selection,	adaptable to complex	hyperparameters;
Methods		crossover, and mutation	spaces.	computationally
	0: 1 . 1	in the solution space.	0. 1.1.1	expensive.
	Simulated	Simulates	Strong global search	Slow convergence;
	Annealing (SA)	thermodynamic cooling	capability; good	sensitive to parameters
		process to escape local	theoretical foundation.	like temperature
T ,	D : C	optima.	0 1 1 0 1	schedule.
Learning-	Reinforcement	Agents learn policies	Suitable for dynamic,	Complex learning
based	Learning (RL)	through interaction with	high-dimensional tasks;	process; low sample
Methods		the environment.	policies are	efficiency; high data
			continuously	demand.
	Doon	Uses neural networks to	improvable. Can handle large	Unatable convergence.
	Deep Reinforcement	represent policies or	state/action spaces;	Unstable convergence; high training cost; lacks
	Learning (Deep	value functions.	highly flexible.	interpretability.
	RL)	value functions.	inginy nexible.	interpretability.
	Graph Neural	Uses graph structure to	Captures inter-task	Complex architecture;
	Networks + RL /	model task dependencies	relationships; suitable	requires graph-based
	Search	and guide	for graph-based	datasets and training.
	Caren	decision-making.	combinatorial	adduces and training.
		accision making.	optimization.	
			opumizanom.	

The training loss comprises three components:

$$\mathcal{L}_{QTRAN} = \mathcal{L}_{TD} + \lambda_1 \mathcal{L}_{opt} + \lambda_2 \mathcal{L}_{nopt}$$

The hyperparameters are $\lambda_1 = 1$ and $\lambda_2 = 0.1$.

(1) TD Loss (consistent with QMIX) :

$$\mathcal{L}_{TD} = (Q_{tot}(s, \mathbf{a}) - y)^2, \quad y = r + \gamma \cdot \max_{\mathbf{a}'} Q_{tot}^{\text{target}}(s', \mathbf{a}')$$

$$\mathcal{L}_{opt} = \left\| Q_{tot}^{\text{joint}}(s, \mathbf{a}) - \sum_{i=1}^{n} Q_{i}(o_{i}, a_{i}) \right\|^{2} \quad \text{for optimal } \mathbf{a}$$

(3) Non-optimality loss:

$$\mathcal{L}_{nopt} = \sum_{i} \left\| Q_{tot}^{\text{joint}}(s, (a^{-i}, a'_{i})) - \sum_{j \neq i} Q_{j}(o_{j}, a_{j}) - Q_{i}(o_{i}, a'_{i}) \right\|^{2}$$

Intuitively, for optimal action combinations, local Q-values should approximate the globally optimal Q; conversely, for non-optimal combinations, they must not exceed the true joint Q.

C.1.4 MF-QMIX. This method replaces QMIX's global state encoder with a mean-field approximation module, which utilizes the average values of neighboring agents as interactive input. Its implementation requires the design of a dynamic graph attention mechanism to accommodate varying numbers of agents and modifications to the experience replay buffer for local observation storage.

In QMIX, each agent's local Q-network primarily considers its own observation o_i and action a_i . MF-QMIX, however, integrates a local mean-field mechanism, enabling each agent's Q-value to perceive the average policy behavior of its neighbors.

Consequently, each agent's Q-network in MF-QMIX is formulated as:

$$Q_i(o_i, a_i, \mu_i)$$

where:

- o_i: local observation of agent i
- a_i : action of agent i
- μ_i : average policy behavior (mean field) of other agents within agent i's neighborhood

The specific form of μ_i is typically:

$$\mu_i = \frac{1}{|N(i)|} \sum_{j \in N(i)} \pi_j(a_j|o_j)$$

For a fully connected structure, this simplifies to:

$$\mu_i = \frac{1}{n-1} \sum_{i \neq i} \pi_j(a_j | o_j)$$

The original QMIX Mixing Network is defined as:

$$Q_{tot} = f(Q_1, Q_2, ..., Q_n; s)$$

In MF-QMIX, the Mixing Network is modified to:

$$Q_{tot} = f(Q_1(o_1, a_1, \mu_1), ..., Q_n(o_n, a_n, \mu_n); s)$$

Specifically, the input to each agent's Q-network is augmented with μ_i , enabling the network to model inter-agent influences and thus improve the representation capability for cooperative group strategies.

C.1.5 CW-QMIX. In its implementation, CW-QMIX preserves QMIX's original value function decomposition structure but incorporates a dynamic weight scheduling mechanism. This mechanism controls the learning weights of different subtasks or samples during training, facilitating curriculum learning. Specifically, when computing the TD loss, samples within the experience replay are assigned a weight ω_i , which is automatically adjusted based on factors such as sample difficulty, training stage, or performance feedback. These dynamic weights can be allocated through a learnable weight network (e.g., a Multi-Layer Perceptron) or heuristic rules, with the weight factor integrated into the training objective:

$$\mathcal{L} = \sum_{i} \omega_{i} \cdot (Q_{tot}(\mathbf{a}_{i}) - y_{i})^{2}$$

C.1.6 OW-QMIX. The central aspect of implementing OW-QMIX lies in adjusting QMIX's TD target term to enhance the efficient utilization of off-policy experiences. OW-QMIX continues to employ QMIX's value function mixing network, but it introduces a weight correction in the target value calculation. This correction accounts for the discrepancy between the behavior policy (behavior distribution) and the target policy, typically achieved using an importance sampling ratio:

$$y_i = r + \gamma \cdot \rho_i \cdot Q_{tot}^{\text{target}}(s', \mathbf{a}')$$
 where $\rho_i = \frac{\pi(\mathbf{a}'|s')}{\mu(\mathbf{a}'|s')}$

- C.1.7 SQIX. Transitioning from QMIX to SQIX can be achieved through three core steps:
 - (1) Replacement of target action selection: QMIX's original target formulation:

$$y = r + \gamma \cdot \max_{\mathbf{a}'} Q_{tot}^{\text{target}}(s', \mathbf{a}')$$

(2) SQIX adopts a softmax-weighted form for the target:

$$y = r + \gamma \cdot \sum_{\mathbf{a}' \in \mathcal{U}} P_{\beta}(\mathbf{a}'|\mathbf{s}') Q_{tot}^{\text{target}}(\mathbf{s}', \mathbf{a}'), \text{ where } P_{\beta}(\mathbf{a}'|\mathbf{s}') \propto \exp(\beta Q_{tot}(\mathbf{s}', \mathbf{a}')), \text{ with parameter } \beta \text{controlling "softness"}.$$

- (3) Definition of joint-subspace \hat{U}^{**} : As discussed in the original paper, this involves selecting only combinations proximate to the current argmax**, such as top-k joint actions, to circumvent exhaustive traversal of the entire action space.
- (4) Update of TD loss: Following the substitution of y, the TD loss continues to be computed as:

$$\mathcal{L} = (Q_{tot} - y)^2$$

while the remaining architectural components are preserved.

C.2 Experiment resullt

Table 8. Comparison of task completion rate across different algorithms.

Dataset	QMIX	CW-QMIX	OW-QMIX	QTRAN	QPLEX	MF-QMIX	SQIX	HoCs-MPQ
Random_1	0.5917	0.5833	0.5917	0.6250	0.6333	0.5667	0.6083	0.7292
BicycleOrder	0.7071	0.7172	0.7172	0.6869	0.7475	0.7272	0.7374	0.8596
TaxiTrajectories	0.4412	0.4314	0.4510	0.4902	0.4706	0.4510	0.4412	0.6735
DidiOrders	0.5882	0.5588	0.6176	0.6765	0.6471	0.6176	0.6176	0.7941

As evidenced by Table 8, our HoCs-MPQ algorithm consistently achieves superior performance across all datasets, demonstrating a significant improvement in task completion rate compared to the benchmark QMIX-based algorithms. This marked advantage underscores the effectiveness of our approach in complex multi-agent scheduling environments.

Crucially, unlike the other evaluated algorithms which are rooted in deep learning and reinforcement learning paradigms, our method does not rely on extensive historical data for model training. Instead, our approach is fundamentally different: it meticulously models the collaborative and conflicting relationships between multiple heterogeneous agents by constructing a weighted undirected graph. Subsequently, it iteratively solves for the maximum weighted independent set within this graph, leveraging a multi-priority queue. This mechanism enables highly efficient collaborative scheduling. This distinct design provides significant advantages, particularly when addressing real-time problems in dynamic disaster scenarios. Learning-based algorithms typically necessitate large volumes of historical data for effective model training, a requirement that is inherently difficult to fulfill in the context of disaster events, which are by nature extreme and often unpredictable occurrences. Furthermore, deep learning and reinforcement learning methods exhibit a strong dependence on the intricate coupling relationships among multiple agents. Consequently, any changes in the number of agents or their online status can lead to a substantial degradation in the model's decision-making efficacy. Our graph-based approach, by contrast, is inherently more robust to such variations, allowing for better adaptability and real-time performance in unpredictable environments.

D Prompt template for interacting with LLM

Prompt Template: Multi-Agent Scheduling for Post-Disaster Perception

Problem Overview: A post-disaster environment requires coordination of three agent types (UAVs, vehicles, and workers) to complete perception tasks at task points and being charged at charge points.

Agents & Locations: Agent Types

- UAVs: Primary task executors requiring periodic charging
- Workers: Task assistants (must collaborate with UAVs)
- Vehicles: Charge assistants (for UAVs)

Location Types

- Task Points: Require UAV and Worker collaboration
- Charge Points: Provide UAV charging via Vehicles

Valid Combinations:

- UAV Stays Put
- Worker Stays Put
- Vehicle Stays Put
- UAV Moves to Task Point
- Worker Moves to Task Point
- UAV Moves to Charge Point
- Vehicle Moves to Charge Point
- Task Execution: UAV + Worker move to Task Point
- Charging Operation: UAV + Vehicle move to Charge Point

Critical Constraints:

- Availability Window: Must operate within agent-specific [up, down] time ranges
- State Dependency: Only idle agents can be scheduled

State Transition Rules: Task Completion:

- Position Update: UAV & Worker move to task point
- Time Cost: max(movement time) + (T_costPow/UAV_speed)

• Power Update: UAV_power -= (movement time + T_costPow)

Charging Completion:

- Position Update: UAV & Vehicle move to charge point
- Time Cost: max(movement time) + (Fullpower current_power)/V_chargePow
- Power Update: UAV_power = Fullpower

Input Data Structure:

- UAV Data: id, x, y, uRge, Fullpower, uPow, U_uptime, U_downtime
- Worker Data: id, x, y, wRge, W_uptime, W_downtime
- Vehicle Data: id, x, y, vRge, V_uptime, V_downtime, V_chargePow
- Task Data: id, x, y, T_costPow
- Charging Data: id, x, y

Optimization Objective:

- Time Horizon: 0-180 units (36 decision points @ 5-unit intervals)
- Primary Goal: Maximize completed tasks while preventing UAV power depletion
- Required Output:
 - a) Scheduling decisions at each interval
 - b) Total completed tasks count

Current System State: [Specific data tables would be inserted here]

Please answer: Which agent-target pairing combination should be prioritized at the current decision interval to maximize task completion while maintaining UAV survivability?

Requirements:

- Choose only ONE combination (Task or Charging)
- Follow analysis steps:
 - Step 1: Determine whether the UAV is performing a task or going to charge.
 - Step 2: Evaluate the assistant (worker, vehicle) situation of the UAVs.
 - Step 3: Select optimal combination based on above priorities
- Final answer must use: <combination>; <combination>; . . .